

T-4515

LOW - FIRING $\text{Pb}(\text{Mg}_{1/3}\text{Nb}_{2/3})\text{O}_3 - \text{PbTiO}_3 - \text{Pb}_5\text{Ge}_2\text{SiO}_{11}$
COMPOSITIONS FOR THICK-FILM CAPACITOR APPLICATIONS

PERMANENT LIBRARY
COLORADO SCHOOL OF MINES
GOLDEN, CO 80401

by
Yangdo Kim

ProQuest Number: 10783973

All rights reserved

INFORMATION TO ALL USERS

The quality of this reproduction is dependent upon the quality of the copy submitted.

In the unlikely event that the author did not send a complete manuscript and there are missing pages, these will be noted. Also, if material had to be removed, a note will indicate the deletion.



ProQuest 10783973

Published by ProQuest LLC (2018). Copyright of the Dissertation is held by the Author.

All rights reserved.

This work is protected against unauthorized copying under Title 17, United States Code
Microform Edition © ProQuest LLC.

ProQuest LLC.
789 East Eisenhower Parkway
P.O. Box 1346
Ann Arbor, MI 48106 – 1346

A thesis submitted to the Faculty and the Board of Trustees of the Colorado School of Mines in partial fulfillment of the requirements for the degree of Master of Science (Materials Science)

Golden, Colorado

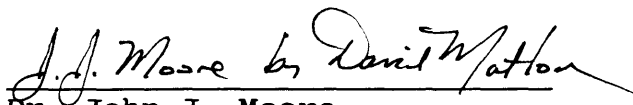
Date: 6/15/94

Signed: 
Yangdo Kim

Approved: 
Dr. Michael J. Haun

Golden, Colorado

Date: 6/15/94


Dr. John J. Moore
Professor and Head,
Department of Metallurgical
and Materials Engineering

ABSTRACT

Commercial ferroelectric thick films have been developed with high dielectric constants for capacitor applications. However, these compositions typically do not densify well at thick film firing temperatures (850 ~ 900°C) and thus require encapsulants to provide environmental stability.

The purpose of this research was to establish the potential of developing $\text{Pb}(\text{Mg}_{1/3}\text{Nb}_{2/3})\text{O}_3$ (PMN) - PbTiO_3 (PT) - $\text{Pb}_5\text{Ge}_2\text{SiO}_{11}$ (PGS) compositions which can densify to closed porosity at typical thick film firing temperatures (850 ~ 900°C) with useful dielectric properties. Crystalline 0.93PMN - 0.07PT powders, which have very high dielectric constant at room temperature, were combined with PGS powders. The PGS melts at $\approx 724^\circ\text{C}$, and thus causes liquid phase sintering of the PMN - PT materials at low temperature.

Reduction in particle size significantly increased the density of fired samples. Bulk samples of PMN - PT with 5 weight percent PGS addition densified to 95 percent of the theoretical density at 850°C. However, greater than 20 weight percent PGS addition is required to densify PMN - PT

at 850°C in thick film form.

The PGS additions to PMN - PT resulted in the formation of lead rich $Pb_3Ge_{2/3}Si_{1/3}O_5$ compared to $Pb_5Ge_2SiO_5$ which was initially added. This phase transformation of PGS caused the perovskite phase to convert to a lead deficient pyrochlore phase. Excess PbO addition to PMN - PT with PGS additions prevented the formation of the pyrochlore phase.

The dielectric constant was reduced by the formation of a diphasic composite of low dielectric constant PGS with high dielectric constant PMN - PT. In bulk samples, the dielectric constant generally increased with increasing firing temperature and time. The dissipation factor slightly increased with increasing PGS addition. Thick film samples of PMN - PT with 30 weight percent PGS and 5 weight percent PbO additions densified to closed porosity firing at 850°C for 10 minutes with a room temperature 1 KHz dielectric constant greater than 1500 and dissipation factor less than 6%. In addition, preliminary results indicate that these compositions are compatible with a commercial silver thick film conductor paste (Dupont 6160).

TABLE OF CONTENTS

| | |
|---|------|
| ABSTRACT | iii |
| TABLE OF CONTENTS | v |
| LIST OF FIGURES | vii |
| LIST OF TABLES | xii |
| ACKNOWLEDGEMENT | xiii |
| CHAPTER 1 : INTRODUCTION | 1 |
| CHAPTER 2 : LITERATURE REVIEW | 4 |
| 2.1 Characteristics of Relaxor Ferroelectric Materials | 4 |
| 2.2 Reaction Mechanisms and Microstructure of Lead Magnesium Niobate (PMN) Based Materials | 7 |
| 2.3 Dielectric Properties of PMN | 12 |
| 2.4 Low-Firing Ceramic Capacitor Compositions | 14 |
| 2.5 Thick Film Capacitor Materials | 15 |
| 2.6 Lead Germanate and Lead Germanium Silicate | 16 |
| CHAPTER 3 : EXPERIMENTAL PROCEDURE | 18 |
| 3.1 Powder Preparation | 18 |
| 3.2 Sample Fabrication | 22 |
| 3.2.1 Bulk Samples | 22 |
| 3.2.2 Thick Film Samples | 23 |
| 3.3 Characterization | 25 |
| 3.3.1 Bulk Properties | 25 |

| | | |
|------------|--|----|
| 3.3.2 | X-Ray Diffraction(XRD) | 26 |
| 3.3.3 | Scanning Electron Microscopy with Energy Dispersive Spectroscopy(SEM-EDS) | 27 |
| 3.4 | Dielectric Measurements | 27 |
| CHAPTER 4 | : RESULT AND DISCUSSION | 29 |
| 4.1 | Bulk Samples | 29 |
| 4.1.1 | Density | 29 |
| 4.1.2 | X-Ray Diffraction(XRD) | 35 |
| 4.1.3 | Microstructural Analysis | 47 |
| 4.1.4 | Dielectric Properties | 53 |
| 4.1.5 | Comparison of Pb_3O_4 and PbO | 59 |
| 4.2 | Thick Film Samples | 67 |
| 4.2.1 | Density | 67 |
| 4.2.2 | X-Ray Diffraction(XRD) | 70 |
| 4.2.3 | Dielectric Properties | 78 |
| CHAPTER 5 | : CONCLUSION | 86 |
| 5.1 | Bulk Samples | 86 |
| 5.2 | Thick Film Samples | 88 |
| CHAPTER 6 | : RECOMMENDATIONS FOR FUTURE RESEARCH | 90 |
| REFERENCES | | 91 |
| APPENDIX | | 95 |

LIST OF FIGURES

| FIGURE | TITLE | PAGE |
|--------|---|------|
| 2.1 | The dielectric constant and dissipation factor versus temperature for PMN | 6 |
| 2.2 | The microstructure of PMN ceramics. The chemical formula of perovskite is $Pb(Mg_{1/3}Nb_{2/3})O_3$ and that of pyrochlore is $Pb_3Nb_4O_{13}$ | 11 |
| 3.1 | Flow chart of the experimental procedure used for fabrication and characterization of the bulk and thick film samples | 19 |
| 4.1 | SEM micrographs of the a) PMN - PT and b) PGS starting powders, ball milled in distilled water for 12 hours with 15 zirconia cylinders | 30 |
| 4.2 | SEM micrographs of the a) PMN - PT and b) PGS starting powders, ball milled in distilled water for 24 hours with 50 zirconia cylinders | 31 |
| 4.3 | The percent theoretical density of pellets from the powders ball milled in distilled water a) for 24 hours with 50 zirconia cylinders and b) for 12 hours with 15 zirconia cylinders plotted versus PGS additions | 33 |
| 4.4 | The percent theoretical density of pellets fired at 850 and 900°C for 1 and 6 hours plotted versus PGS additions | 34 |
| 4.5 | The percent theoretical density of PMN - PT pellets with 0, 5, and 20 weight percent PGS additions fired for 1 hour plotted versus temperature | 36 |
| 4.6 | The percent theoretical density of PMN - PT pellets with 0, 5, and 20 weight percent PGS additions fired at 850°C plotted versus time | 37 |

- 4.7 X-ray diffraction patterns of PMN - PT powders A) prepared from Pb_3O_4 and B) from PbO calcined at $800^\circ C$ for 4 hours one and two times. The peaks in the top pattern are labeled with P for PMN - PT perovskite, L for lead oxide, and Pyro for $Pb_3Nb_2O_8$ pyrochlore 38
- 4.8 X-ray diffraction patterns of PMN - PT samples, prepared from Pb_3O_4 , fired at 850, 900, and $1200^\circ C$ for 1 hour. The peaks in the top pattern are labeled with P for PMN - PT perovskite and Pyro for $Pb_3Nb_4O_{13}$ pyrochlore 40
- 4.9 X-ray diffraction patterns of PMN - PT samples, prepared from PbO, fired 850, 900, and $1200^\circ C$ for 1 hour. The peaks in the top pattern are labeled with P for PMN - PT perovskite and Pyro for $Pb_3Nb_4O_{13}$ pyrochlore 41
- 4.10 X-ray diffraction patterns of PMN - PT samples A) prepared from Pb_3O_4 and B) from PbO fired at 850 and $900^\circ C$ for 6 hours. The peaks in the top pattern are labeled with P for PMN - PT perovskite and Pyro for $Pb_3Nb_4O_{13}$ pyrochlore 42
- 4.11 The percent pyrochlore phase in pellets fired at $850^\circ C$ plotted versus time 43
- 4.12 The percent pyrochlore phase in pellets fired for 1 hour plotted versus temperature 44
- 4.13 X-ray diffraction patterns of calcined ($800^\circ C$ for 4 hours) PMN - PT powder, and PMN - PT with 20wt% PGS addition fired at $900^\circ C$ for 6 hours. The peaks are labeled with P for PMN - PT perovskite, L for lead oxide, and Q for the $Pb_3Ge_{2/3}Si_{1/3}O_5$ 46
- 4.14 SEM micrographs of the fracture surface of pellets fired at $850^\circ C$ for 1 hour; a) PMN - PT b) PMN - PT with 5wt% PGS addition c) PMN - PT with 20wt% PGS addition 48
- 4.15 SEM micrographs of the fracture surface of pellets fired at $850^\circ C$ for 6 hours; a) PMN - PT b) PMN - PT with 5wt% PGS addition c) PMN - PT with 20wt% PGS addition 49

4.16 SEM micrographs of the fracture surface of pellets fired at 900°C for 1 hour; a) PMN - PT b) PMN - PT with 5wt% PGS addition c) PMN - PT with 20wt% PGS addition 50

4.17 SEM micrographs of the fracture surface of pellets fired at 900°C for 6 hours; a) PMN - PT b) PMN - PT with 5wt% PGS addition c) PMN - PT with 20wt% PGS addition 51

4.18 SEM micrographs of a crack inside a pellet of PMN - PT fired at 900°C for 6 hours; a) cross - section, and b) surface of the crack 52

4.19 The dielectric constant and dissipation factor of a PMN - PT pellet fired at 900°C for 6 hours plotted versus temperature for five frequencies 54

4.20 Temperature dependence of the dielectric constant and dissipation factor at 1 KHz of PMN - PT pellets fired at 850 and 900°C for 1 and 6 hours 55

4.21 Temperature dependence of the dielectric constant and dissipation factor at 1 KHz for PMN - PT with and without PGS additions fired at 900°C for 6 hours 56

4.22 The measured dielectric constant of samples fired at 900°C for 6 hours plotted versus PGS addition, compared with calculating based on the series and parallel dielectric mixing models 58

4.23 Change in capacitance ($\Delta C/C$) of samples fired at 850°C for 1 hour plotted versus temperature 61

4.24 Change in capacitance ($\Delta C/C$) of samples fired at 900°C for 6 hours plotted versus temperature 62

4.25 The temperature dependence of the dielectric constant and dissipation factor of PMN - PT pellets fired at 900 and 1200°C for 1 hour, comparing the use of Pb_3O_4 and PbO raw materials 64

- 4.26 SEM micrographs of the fractured cross sections of thick film samples fired at 850°C for 3 hours with a heating rate of 3.33°C/min; a) PMN - PT + 5wt% PGS b) PMN - PT + 20wt% PGS c) PMN - PT + 40wt% PGS. The thick film layers are shown on the top of the photos with the alumina substrate on the bottom 68
- 4.27 SEM micrographs of the fractured cross sections of thick film samples fired at 850°C for 10 minutes with a heating rate of 580°C/min; a) PMN - PT + 20wt% PGS + 5wt% PbO b) PMN - PT + 30wt% PGS + 5wt% PbO. The thick film layers are shown on the top of the photos with the alumina substrate on the bottom 69
- 4.28 SEM micrographs of the fractured cross sections of thick film samples fired at 850°C for 10 minutes with a heating rate of 580°C/min; a) PMN - PT + 5wt% PbO b) PMN - PT + 10wt% PbO c) PMN - PT + 20wt% PbO. The thick film layers are shown on the top of the photos with the alumina substrate on the bottom 71
- 4.29 X-ray diffraction patterns of the surface of PMN - PT + 30wt% PGS thick film samples fired at 800, 850, and 900°C for 10 minutes with a heating rate of 580°C/min. The peaks in the top pattern are labeled with P for PMN - PT perovskite, and Pyro for $Pb_3Nb_4O_{13}$ pyrochlore 72
- 4.30 X-ray diffraction patterns of the surface of PMN - PT + 30wt% PGS thick film samples fired at 850°C for 10, 30. and 60 minutes with a heating rate of 580°C/min. The peaks in the bottom pattern are labeled with P for PMN - PT perovskite, and Pyro for $Pb_3Nb_4O_{13}$ pyrochlore in the top pattern 74
- 4.31 X-ray diffraction patterns of the surface of PMN - PT + 30wt% PGS thick film samples fired at 850°C for 10 minutes with a heating rate of 3.33°C/min, 100°C/min, and 580°C/min. The peaks in the top pattern are labeled with P for PMN - PT perovskite, and Pyro for $Pb_3Nb_4O_{13}$ pyrochlore 75

4.32 X-ray diffraction patterns of the surface of PMN - PT with 0, 5, 20, and 30wt% PGS addition thick film samples fired at 900°C for 10 minutes with a heating rate of 580°C/min. The peaks in the top pattern are labeled with P for PMN - PT perovskite, and Pyro for $Pb_3Nb_4O_{13}$ pyrochlore 76

4.33 X-ray diffraction patterns of the surface of PMN - PT + 30wt% PGS + 5wt% PbO thick film samples fired at 850°C for 10 and 30 minutes with a heating rate of 580°C/min. The peaks in the top pattern are labeled with P for PMN - PT perovskite, and Pyro for $Pb_3Nb_4O_{13}$ pyrochlore 77

4.34 The dielectric constant and dissipation factor of a thick film sample of PMN - PT with 30wt% PGS and 5wt% PbO fired at 850°C for 10 minutes with a heating rate of 580°C/min plotted versus temperature for five frequencies 79

4.35 SEM micrographs of a fractured cross section of a thick film samples of PMN - PT with 30wt% PGS and 5wt% PbO fired at 850°C for 10 minutes with a heating rate of 580°C/min. The thick film dielectric layer is shown on the top of the photo with the Pt conductor shown at the bottom of the dielectric layer 80

4.36 SEM micrographs of the fractured cross sections of thick film PMN - PT with 30wt% PGS and 5wt% PbO samples fired at 850°C for 10 minutes with a heating rate of 580°C/min; a) fired with silver electrode (Dupont 6160) b) fired with silver/palladium electrode (Dupont 6134) . . . 83

4.37 The dielectric constant and dissipation factor of a PMN - PT with 30wt% PGS and 5wt% PbO thick film sample fired with silver electrode (Dupont 6160) at 850°C for 10 minutes with a heating rate of 580°C/min plotted versus temperature for five frequencies 85

LIST OF TABLES

| TABLE | TITLE | PAGE |
|-------|--|------|
| 4.1 | The effect of PGS addition on the dielectric constant, transition temperature, and density of the samples heat treated at 850 and 900°C for 1 and 6 hours | 60 |
| 4.2 | The TCC categories of the PMN - PT samples with 0, 5, and 20wt% PGS additions heat treated at 850 and 900°C for 1 and 6 hours | 63 |
| 4.3 | Comparison of the resulting properties of PMN - PT pellets prepared with Pb_3O_4 and PbO raw materials | 65 |
| 4.4 | The summary of the densification behavior and electrical properties of four different thick film compositions fired at 850°C for 10 minutes with a heating rate of 580°C/min | 82 |

ACKNOWLEDGEMENT

I would like to express my gratitude to Dr. Michael J. Haun to whom I am deeply indebted professionally and personally for guiding me in the completion of my thesis research.

I wish to extend my sincere thanks to my committee members: Dr. John J. Moore and Dr. Dennis W. Readey for their general support in conducting this study.

I wish to thank all my fellow colleagues and friends, who have shared their lives with me, for their friendship.

I am also greatly appreciative for the support and understanding I received from my sisters and brothers'-in-law.

By far my greatest appreciation goes to my grandmother and mother for their love.

CHAPTER 1

INTRODUCTION

The development of ceramic capacitors with small size, high capacitance, electrical stability, and low cost have become increasingly important in the microelectronic industry.¹ For these reasons, lead-based relaxor ferroelectric compositions have been developed for multilayer capacitor applications with high dielectric constant and low-firing temperature.¹⁻¹⁰ However, these relaxor ferroelectric compositions have limited use in thick film form, because of poor densification which results in the need for encapsulants to provide environmental stability.

Recently, low-firing thick film dielectrics based on lead iron niobate and lead iron tungstate with high dielectric constant have been developed.⁸⁻¹⁰ These thick film dielectrics densify through liquid phase sintering with a fluxing agent such as $\text{Bi}_2\text{O}_3/\text{Li}_2\text{O}$, PbO/WO_3 , PbO etc, however these compositions do not densify to closed porosity in thick film form. The main purpose of this research is to

establish the potential of developing low-fire ferroelectric compositions with useful dielectric properties by liquid phase sintering of the $0.93\text{Pb}(\text{Mg}_{1/3}\text{Nb}_{2/3})\text{O}_3$ (PMN) + 0.07PbTiO_3 (PT) materials with $\text{Pb}_5\text{Ge}_2\text{SiO}_{11}$ (PGS) additions for thick film capacitor applications.

The PMN - PT solid solution and PGS were selected for this work based on their unique properties. The $0.93\text{PMN} + 0.07\text{PT}$ solid solution has a very high dielectric constant ($\geq 20,000$) at room temperature.¹¹ Lead germanium silicate (PGS) is a potential candidate for use as a sintering aid to lower the processing temperatures of dielectric materials for capacitor applications. This is because PGS is ferroelectric and has a low melting temperature ($\approx 724^\circ\text{C}$). In addition, PGS can be easily formed into glass due to the presence of the glass formers GeO_2 and SiO_2 .¹² PGS has a high dielectric constant, even in glass form compared to most other glass compositions.

For this research, samples were prepared in both bulk and thick film forms to investigate the densification behavior, microstructural development, and resulting dielectric properties of compositions in the PMN - PT/PGS system. The density was measured by the Archimedes method for bulk samples and estimated by SEM for thick film samples. The microstructure of each sample was evaluated by

SEM. X-ray diffraction was utilized for crystal phase analyses. The dielectric properties were measured as a function of temperature and frequency using a computer automated system.

The thesis consists of six chapters. This introductory chapter provides the background on the thesis research topic, and purpose of the research work. Chapter 2 is a literature review of topics relevant to the subject area of the research. Chapter 3 presents the equipment and procedures employed in the research conducted. Chapter 4 provides the results of the physical and electrical properties. Chapter 5 presents the conclusions of the research. Finally, chapter 6 recommends future work.

CHAPTER 2

LITERATURE REVIEW

This chapter is divided into six sections. In the first three sections, the characteristics of relaxor ferroelectrics and lead magnesium niobate perovskite materials are reviewed. The fourth and fifth sections discuss general trends of the electronics industry and the development of low-temperature cofired ceramics for capacitor applications. In the final section, the unique properties of lead germanate and lead germanium silicate materials as sintering aids are presented.

2.1 Characteristics of Relaxor Ferroelectric Materials

Ferroelectrics are characterized as crystals that possess a spontaneous dipole, and this dipole can be rotated by the applying an AC electric field. Normally, ferroelectric materials show a sharp increase in the dielectric constant at the Curie temperature due to the phase transition from an unpolarized to a polarized state.¹³

Relaxor ferroelectrics¹⁴ have a diffuse phase transition where a broad phase transition region occurs rather than a sharp phase transition exhibited by normal ferroelectrics. In addition, the maxima of the dielectric constant and dissipation factor are strongly frequency dependent, and this maxima shifts toward a high temperature with increasing frequency. Lead magnesium niobate ($\text{Pb}(\text{Mg}_{1/3}\text{Nb}_{2/3})\text{O}_3$, PMN) is the most investigated relaxor ferroelectric. Figure 2.1 shows the dielectric constant and dissipation factor versus temperature at various frequencies for PMN without PT addition.¹⁵ This figure illustrates the broad frequency dependent behavior of the dielectric properties at the ferroelectric to paraelectric phase transition which characterizes relaxor ferroelectrics.

The cause of the diffuse phase transition has been widely investigated under different conditions. Smolenskii et al.¹⁶ reported that the diffuse phase transition is related to the compositional fluctuation at the B-site of the perovskite ABO_3 structure. More than one type of ion could randomly occupy the crystallographical equivalent site. The random distribution of ions at the same site generates different microregions which have different Curie temperatures, which causes a broad phase transition.

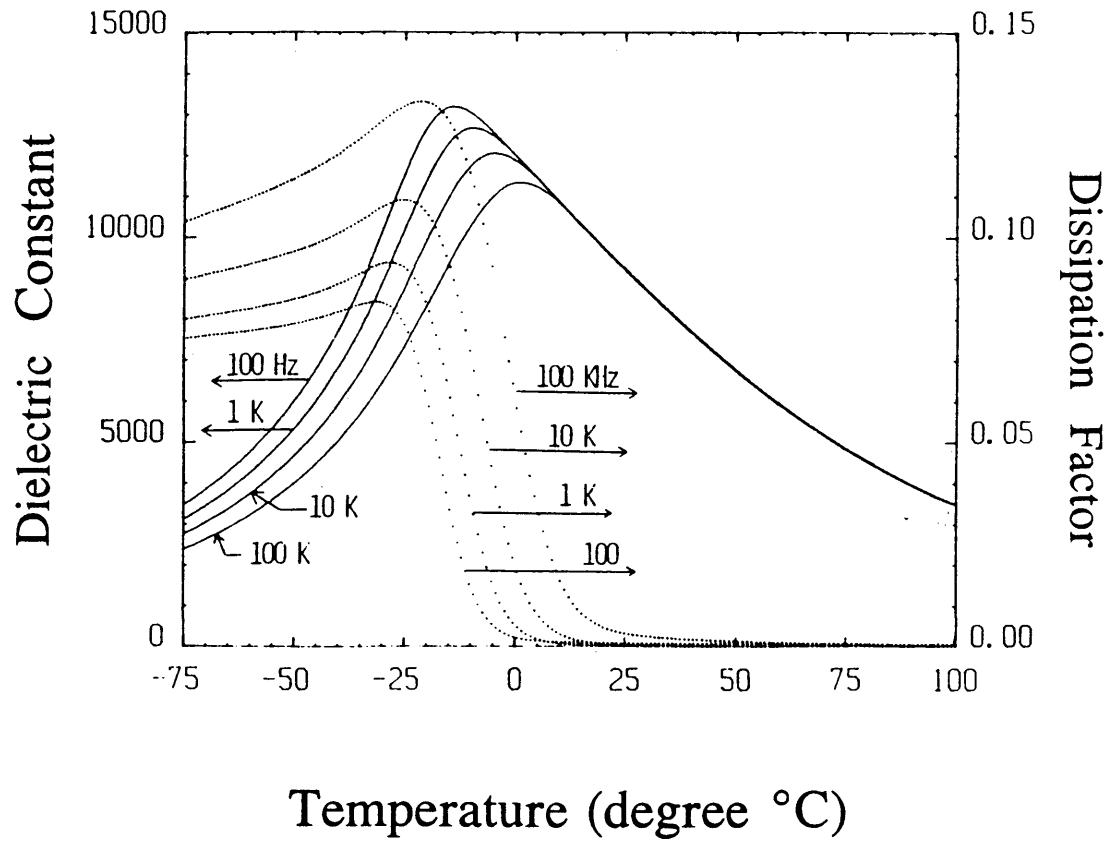


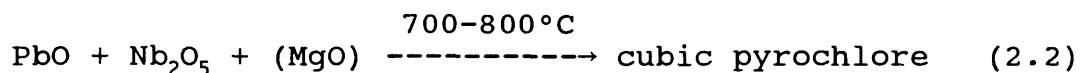
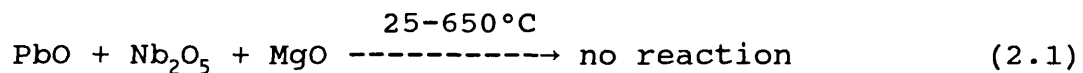
Figure 2.1 The dielectric constant and dissipation factor versus temperature for PMN.¹⁵

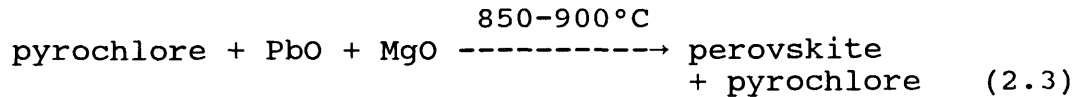
The broadness of the transition point depends on the randomness of the B-site cations on the microscale. N. Setter and L. E. Cross^{17,18} have shown that the diffuse transition is sharpened by the increase in the degree of ordering of the B-site cations in relaxor ferroelectrics. The degree of ordering was controlled by varying the thermal treatment.

2.2 Reaction Mechanisms and Microstructure of Lead Magnesium Niobate (PMN) Based Materials

Among the relaxor ferroelectrics, lead magnesium niobate is the most widely investigated, because of the excellent dielectric and ferroelectric properties. PMN was first synthesized and investigated by Smolenskii and Agronovskaya in the late 1950s.¹⁹

S. L. Swartz and T. R. Shrout²⁰ investigated the reaction kinetics of the formation of perovskite PMN from conventional reaction of mixed oxides. They proposed the following reaction sequence.





There were no reactions up to approximately 650°C. The cubic pyrochlore ($\text{Pb}_3\text{Nb}_4\text{O}_{13}$) phase started to form by 700°C. As the temperature was further increased, the amount of cubic pyrochlore phase increased with a decrease in niobium oxide. The perovskite PMN ($\text{Pb}(\text{Mg}_{1/3}\text{Nb}_{2/3})\text{O}_3$) first started to appear at 850°C. The formation of perovskite PMN took place until 950°C, and the reaction was complete at this temperature.

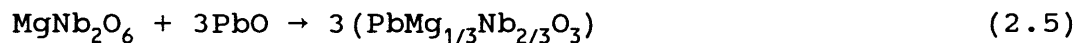
S. L. Swartz and T. R. Shrout²⁰ found that the yield of perovskite phase was increased by increasing the calcine temperature. However, there was still a relatively large amount of parasitic pyrochlore phase even after calcining at high temperatures. They found that the yield of perovskite could not be considerably increased, even by increasing the calcining time to longer than four hours. They also found that the reaction (Equation 2.3) was incomplete, as indicated by the detection of excess lead and magnesium oxides.

To minimize the formation of the pyrochlore phase, two new fabrication processes were developed,²⁰⁻²² which were characterized by prereacting two of the single oxide

17
APR 1963

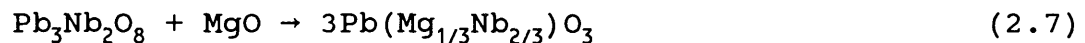
components during the first of two calcination steps.

The first process developed consists of prereacting MgO and Nb₂O₅ to form columbite MgNb₂O₆²⁰, which has a structure similar to perovskite. The MgNb₂O₆ is then reacted with PbO to form perovskite PMN. In this method, the formation of the intermediate pyrochlore phase is eliminated by the following reactions.



To form the parasitic pyrochlore phase requires Nb₂O₅ to first be liberated from MgNb₂O₆, and then reacted with PbO. However, the reaction kinetics of this process are slow, and thus the formation of pyrochlore can be neglected.

Another process that has been used involves prereacting PbO and Nb₂O₅ to form Pb₃Nb₂O₈.²² This Pb₃Nb₂O₈ is then reacted with MgO. The overall reaction sequence is as follows:



In the second reaction step(Equation 2.7) no free PbO

is involved, and hence the volatilization problem of PbO is reduced.

The addition of excess MgO further reduces the formation of the pyrochlore phase and lowers the calcining temperature.^{20,23} The increase of the partial pressure of oxygen during calcining has also been shown to affect the formation of the pyrochlore phase.²⁴ By using solution-derived MgNb_2O_6 , the calcining temperature has been further reduced.²⁵

E. Goo et al.²⁶ studied the microstructure of PMN ceramics by using transmission electron microscopy (TEM) and energy dispersive x-ray spectroscopy (EDS). For this investigation ceramic samples were processed by both mixed oxides and precalcining methods to have the same volume fraction of pyrochlore phase. Figure 2.2 shows the proposed microstructural model. MgO inclusions were found in perovskite PMN grains with rectangular shaped pyrochlore phases in a PbO matrix. As seen in Figure 2.2, MgO is surrounded by the perovskite grains, which prevents the reaction of MgO and pyrochlore to form the perovskite phase. This microstructural model explains why the addition of excess MgO has been found^{20,23} to assist in reducing the pyrochlore phase. These results also help to understand why excess PbO additions have not been found^{20,23} to reduce the

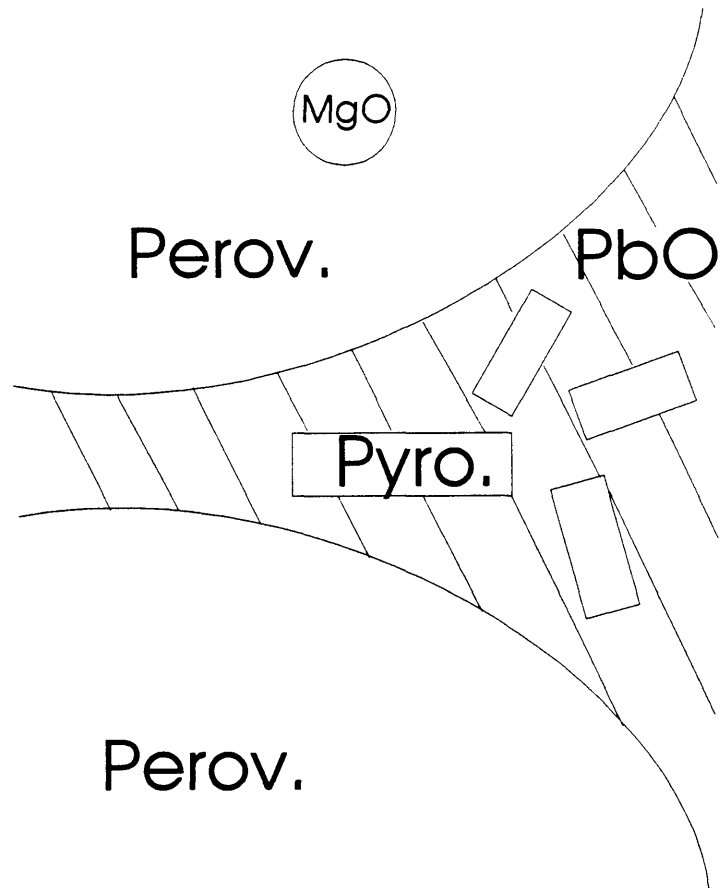


Figure 2.2 The microstructure of PMN ceramics.²⁶
The chemical formula of perovskite is $\text{Pb}(\text{Mg}_{1/3}\text{Nb}_{2/3})\text{O}_3$ and that of pyrochlore is $\text{Pb}_3\text{Nb}_4\text{O}_{13}$.

amount of the pyrochlore phase. However, PbO addition was found to assist in densification through liquid phase sintering.²⁶

2.3 Dielectric Properties of PMN

The dielectric properties of PMN materials have been widely investigated over the last three decades in both single crystal²⁷ and polycrystalline^{19,28,29} ceramic forms. The maximum dielectric constant of PMN at 1 KHz is about 12,000 for polycrystalline ceramic (see Figure 2.1), and about 20,000 in single crystal form. The temperature of maximum dielectric constant is around -12°C, which is higher than that of the dissipation factor maximum ($\approx -35^\circ\text{C}$).

The dielectric properties of PMN polycrystalline ceramics are dominated by the grain boundary phases.^{11,30-32} This is because the high dielectric constant perovskite PMN grains are continuously or semi-continuously connected with an amorphous low dielectric constant grain boundary. The grain boundary effect can be reduced by increasing the grain size of the perovskite PMN. This grain size dependency of the dielectric properties of PMN materials has been widely investigated.^{11,30-32}

Generally, a polycrystalline ceramic microstructure is a mixture of parallel and series connected intergranular

boundaries. C. A. Randall et. al.¹¹ derived the following dielectric mixing law for this type of microstructure based on the relationship between the series mixing of the single crystal and grain boundary dielectric constants.

$$\frac{1}{\bar{K}_{\max}} = \frac{1}{K_{\max}^x} + \frac{1}{R} \cdot \frac{1}{K^{gb}} \quad (2.8)$$

\bar{K}_{\max} = Maximum dielectric constant of the ceramic relaxor.

K^{gb} = Dielectric constant of grain boundary

K_{\max}^x = Maximum dielectric constant of single crystal relaxor

$$R = \langle t^g \rangle / \langle t^{gb} \rangle$$

$\langle t^g \rangle$ = mean grain size.

$\langle t^{gb} \rangle$ = mean grain boundary thickness.

As seen by Equation (2.8), the dielectric constant values increase with increasing grain size. The grain size can be controlled by sintering temperature. Normally, as the sintering temperature is increased, the grain size and the resulting dielectric constant are increased.³² However,

long calcining times may decrease the dielectric constant, because of volatilization of PbO which results in the formation of more pyrochlore phase.

2.4 Low-Firing Ceramic Capacitor Compositions

Recently, the development of ceramic capacitors with small size, high capacitance, electrical stability, and low cost have become increasingly important in the microelectronic industry.¹ Modified BaTiO₃ ceramic compositions have been widely used as ceramic capacitor materials with high dielectric constant. However, these materials generally require high firing temperatures (>1300°C), and thus in multilayer form expensive noble metal internal electrodes are required which can stand high sintering temperatures.² Unfortunately, these metals may constitute over half of the manufacturing cost of the capacitor.¹

For these reasons, great efforts have been made to lower the processing temperatures of dielectric materials for capacitor applications. This can be achieved by introducing sintering aids which allow the use of a less-expensive internal electrode material such as Ag or Ag/Pd alloy.¹

In recent years, lead-based relaxor ferroelectrics have

been developed for capacitor applications with high dielectric constant and low-firing temperature.¹⁻¹⁰ Yonezawa³ reported that $\text{Pb}(\text{Zn}_{1/3}\text{Nb}_{2/3})\text{O}_3 - \text{Pb}(\text{Fe}_{1/2}\text{Nb}_{1/2})\text{O}_3 - \text{Pb}(\text{Fe}_{2/3}\text{W}_{1/3})\text{O}_3$ compositions can be fired at 870°C with a dielectric constant of 14,500 and a dissipation factor of 0.45%. Currently six Japanese companies are commercializing relaxor based multilayer ceramic capacitors.³³

2.5 Thick-Film Capacitor Materials

A general trend in microelectronic circuitry is the integration of a variety of passive components such as resistors, inductors, and capacitors to reduce processing cost and improve volumetric efficiency.^{34,35} Conventionally, discrete multilayer chip capacitors have been used for hybrid microcircuit applications. Thick film capacitor materials have been developed, but have limited use because of poor densification behavior which results in the need for encapsulants to provide environmental stability.

As discussed in the last section lead-based relaxor compositions are promising for low fire capacitor applications.¹⁻¹⁰ However, in thick film form, these materials typically do not densify well.³⁶ Recently, low-firing thick film dielectrics based on lead iron niobate and lead iron tungstate with high dielectric constant have been

developed.⁸⁻¹⁰ These thick film dielectrics densify through the liquid phase sintering with a fluxing agent such as $\text{Bi}_2\text{O}_3/\text{Li}_2\text{O}$, PbO/WO_3 , PbO etc. T. Yasumoto⁹ et al. reported that the $(\text{Pb}_{0.95}\text{Ba}_{0.05})[(\text{Fe}_{1/2}\text{Nb}_{1/2})_{0.95}(\text{Cu}_{1/2}\text{W}_{1/2})_{0.05}]\text{O}_3$ composition with nine weight percent PbO/WO_3 (85.2/14.8 weight ratio) fluxing agent was fired at 900°C with a dielectric constant of 12,500 at 25°C and a dissipation factor of 0.5%. However, these compositions do not densify to closed porosity in thick film, and thus probably require encapsulants for environmental stability.

2.6 Lead Germanate and Lead Germanium Silicate

Lead germanate ($\text{Pb}_5\text{Ge}_3\text{O}_{11}$) and lead germanium silicate ($\text{Pb}_5(\text{Ge}_{1-x}\text{Si}_x)_3\text{O}_{11}$) are unusual ferroelectric crystals, because these compositions can be easily formed into glass, due to the presence of the glass formers GeO_2 and SiO_2 . Also, these compositions have low melting temperatures ($\leq 738^\circ\text{C}$). These compositions are promising candidates for sintering aids to lower the processing temperatures of dielectric materials for capacitor and piezoelectric applications.¹²

Lead germanium and silicon containing compounds have been investigated as a sintering aids in a variety of compositions.^{1,6,7,12,37-40} Crystalline $\text{Pb}_5\text{Ge}_3\text{O}_{11}$ has been added to PLZT¹², PZT³⁷, BaTiO_3 ³⁸ and $\text{Pb}(\text{Fe}_{2/3}\text{W}_{1/3})\text{O}_3$ - $\text{Pb}(\text{Fe}_{1/2}\text{Nb}_{1/2})\text{O}_3$ ¹

to permit liquid phase sintering at low temperatures. Lead germanium silicate compositions have also been used to reduce the sintering temperature.^{6,7,39}

S. J. Jang et al.¹ reported that $\text{Pb}(\text{Fe}_{2/3}\text{W}_{1/3})\text{O}_3$ - $\text{Pb}(\text{Fe}_{1/2}\text{Nb}_{1/2})\text{O}_3$ solid-solution could be fired below 850°C with the addition of $\text{Pb}_5\text{Ge}_3\text{O}_{11}$ and cofired with pure Ag electrode.

CHAPTER 3

EXPERIMENTAL PROCEDURE

The experimental procedures and equipment utilized in this work are described in the four sections of this chapter, which cover the powder preparation method, fabrication of bulk and thick film samples, and microstructural and property characterization. Figure 3.1 shows the flow chart of the experimental procedure used in this research.

3.1 Powder Preparation

The compositions of the materials used for this research were $0.93\text{Pb}(\text{Mg}_{1/3}\text{Nb}_{2/3})\text{O}_3 - 0.07\text{PbTiO}_3$ solid solution and $\text{Pb}_5\text{Ge}_2\text{SiO}_{11}$. These compositions were selected based on their unique properties. The $0.93\text{Pb}(\text{Mg}_{1/3}\text{Nb}_{2/3})\text{O}_3 - 0.07\text{PbTiO}_3$ (PMN - PT) composition has a high dielectric constant ($\geq 20,000$) at room temperature.¹¹ The addition of seven mole percent lead titanate, with a Curie temperature T_c of 492°C , increases the T_c to approximately 23°C compared to -12°C for pure PMN. The $\text{Pb}_5\text{Ge}_2\text{SiO}_{11}$ composition has a low melting

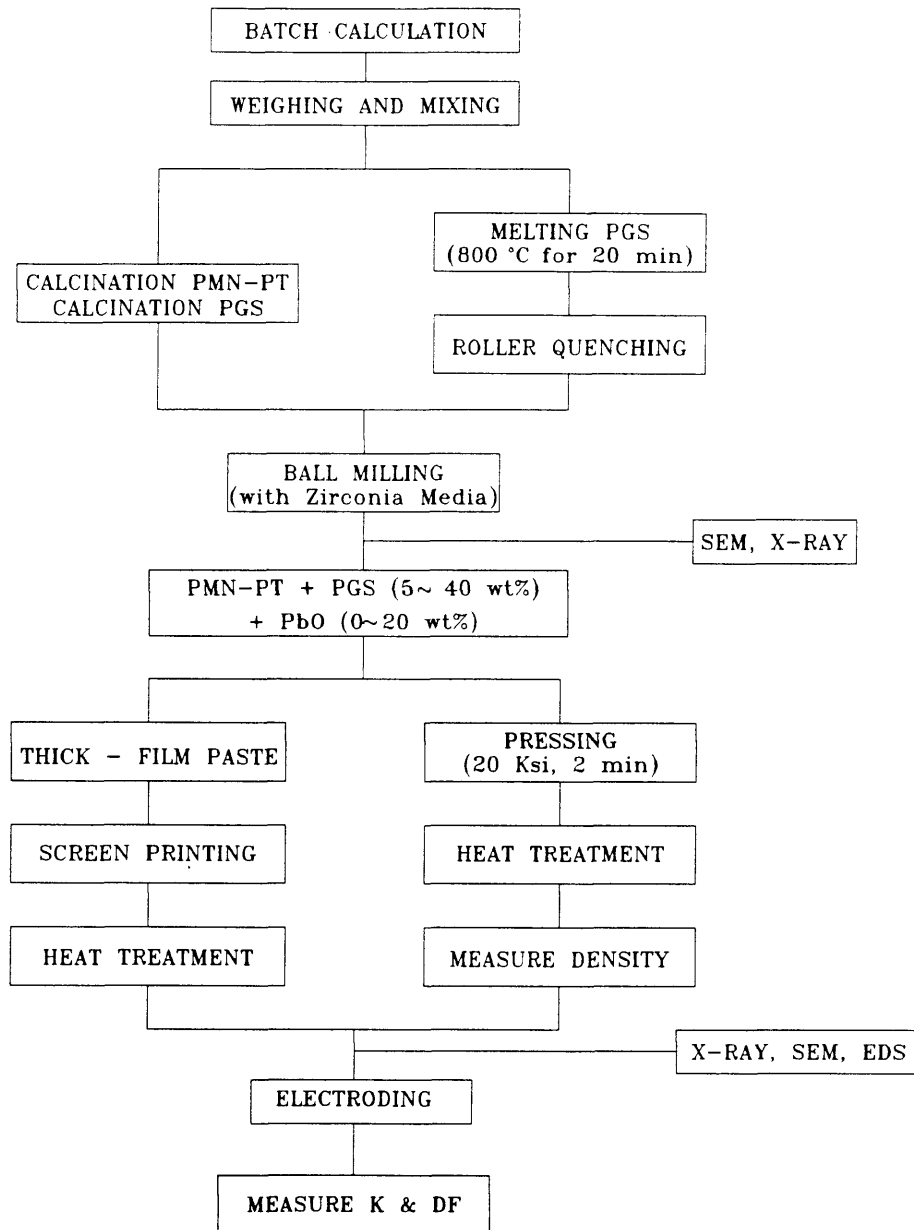


Figure 3.1 Flow chart of the experimental procedure used for fabrication and characterization of the bulk and thick film samples.

temperature ($\approx 724^\circ\text{C}$), and is easily formed into glass because of the presence of the glass formers GeO_2 and SiO_2 .

The precalcining technique (discussed in Section 2.2) was used to prepare the $0.93\text{Pb}(\text{Mg}_{1/3}\text{Nb}_{2/3})\text{O}_3 - 0.07\text{PbTiO}_3$ solid solution composition.²⁰ This procedure consists of two steps. The first step involves the precalcining of MgO and Nb_2O_5 to form columbite (MgNb_2O_6). The second step involves the formation of perovskite ($0.93\text{Pb}(\text{Mg}_{1/3}\text{Nb}_{2/3})\text{O}_3 - 0.07\text{PbTiO}_3$) solid solution by reacting Pb_3O_4 (or PbO), TiO_2 , and MgNb_2O_6 together. Separate batches with Pb_3O_4 and PbO were made (see Section 4.1.5 for a comparison of the resulting properties). Five weight percent excess MgO was initially calcined with the Nb_2O_5 , because excess MgO has previously been shown to increase the formation of perovskite.^{20,23}

The starting raw materials were reagent grade oxides Pb_3O_4 , PbO , MgO , Nb_2O_5 , TiO_2 and SiO_2 , and electronic grade GeO_2 . These materials were first heated at 150°C for one hour to evaporate moisture, and then weighed based on the batch calculations.

Based on the batch calculation, MgO and Nb_2O_5 were mixed and milled in a 125 ml nalgene bottle with zirconia media and distilled water for 12 hours. This mixture was then dried in the oven at 100°C . After drying, the solid mass was crushed with a mortar and pestle, and then dry ball

milled with zirconia media for 5 hours to obtain a homogeneous mixture. This mixture was calcined in a covered alumina crucible at 1200°C for 2 days. A heating rate of 10°C/min was used with the cooling rate controlled by turning the power off to the furnace. X-ray diffraction (XRD) was used to confirm the formation of columbite (MgNb_2O_6).

Based on the batch calculation, Pb_3O_4 (or PbO) and TiO_2 were mixed with columbite (MgNb_2O_6) powder and milled in a 125 ml nalgene bottle with zirconia media and distilled water for 12 hours. This mixture was then dried in an oven at 100°C. After drying, the solid mass was crushed with a mortar and pestle, and then dry ball milled with zirconia media for 5 hours to obtain a homogeneous mixture. The mixture was calcined at 800°C for 4 hours with a heating rate of 3.33°C/min and natural cooling in the furnace. XRD was used to confirm the formation of the perovskite phase. This calcined powder was ball milled in distilled water for 24 hours, and then sieved through a 325 mesh (45 μm) screen.

The $\text{Pb}_5\text{Ge}_2\text{SiO}_{11}$ powder was prepared in both glass and crystalline forms. The Pb_3O_4 , SiO_2 , and GeO_2 powder were weighed based on the batch calculation, and dry mixed with zirconia balls for 12 hours in a 125 ml nalgene bottle. To prepare the glass powder, this mixture was then placed in a

covered platinum crucible, and melted at 800°C for 20 minutes. The liquid was poured into counter rotating steel rollers of a twin-roller quenching apparatus to form amorphous ribbon. Before pouring the liquid, the steel rollers were cooled with liquid nitrogen to increase the quenching rate. This glass ribbon was ball milled with zirconia media in distilled water for 24 hours. The mixture was then poured through a 325 mesh (45 μ m) sieve, and dried in an oven at 100°C. To prepare the crystal powder, the mixture (discussed above) was placed in a covered platinum crucible, and calcined at 700°C for 6 hours. This calcined powder was ball milled in distilled water for 24 hours, and then sieved through a 325 mesh (45 μ m) screen. XRD was used to identify the phases present.

3.2 Sample Fabrication

3.2.1 Bulk Samples

The 0.93Pb(Mg_{1/3}Nb_{2/3})O₃ - 0.07PbTiO₃ solid solution powder was mixed with 5, 10, and 20 weight percent Pb₅Ge₂SiO₁₁ powder. These powders were mixed in a 125 ml nalgene bottle with 50 zirconia balls and distilled water for 12 hours, and then dried in an oven at 100°C.

These PMN - PT mixtures were pressed into pellets without binder with a pressure of 20Ksi held for two minutes

in a 10 mm steel die. The pellets were fired on platinum foil in a covered alumina crucible at 850 to 1200°C with hold times from 1 to 6 hours. To control the volatility of lead oxide during firing, a mixture of PbO and ZrO₂ with a 70 to 30 weight percent ratio was placed in a small alumina crucible and included in the large crucible with the pellets during firing.

3.2.2 Thick Film Samples

The 0.93Pb(Mg_{1/3}Nb_{2/3})O₃ - 0.07PbTiO₃ solid solution powder with 5, 20, 30, and 40 weight percent Pb₅Ge₂SiO₁₁ additions were prepared as described above. These powders were mixed with organic vehicle in a seven to three (inorganic to organic) weight ratio. The organic vehicle consisted of a nine to one weight ratio of pine oil* and ethyl cellulose.** These pastes were manually mixed with a glass rod. The mixing was conducted three times with 24 hours between mixing steps to increase the homogeneity of the final paste.

These pastes were screen printed on polycrystalline 96

* Technal Ltd., Product No. P123, 708 North Texas Rd., Anacortes, WA, 98221.

** Aldrich Chemical Company, Inc., Product No. 24749-9, 1001 W. Saint Paul Ave., Milwaukee, WI, 53233.

percent alumina thick film substrates.*** Before screen printing the dielectric paste, an electrode consisting of pure platinum thick film paste (Dupont 9894) was screen printed and fired at 1300°C for one hour. This provided the bottom electrode for dielectric measurement. A DEK Model 250 screen printer and 200 mesh screen were used.

One layer of dielectric paste was screen printed and then dried at 150°C for 10 minutes. A second dielectric layer was printed on top of the first layer and dried. These two layers were then cofired with the alumina substrate placed on platinum foil in a covered alumina crucible. This procedure was repeated four additional times to produce a total of 10 dielectric layers to reduce defects such as pin-holes. The samples were fired at 800 to 1200°C with a hold time from 10 minutes to 6 hours depending on the samples. To control the volatility of lead oxide during firing in the box furnace a similar procedure as that used for bulk samples was utilized. A rapid thermal annealing furnace was also used to fire the thick film samples to reduce the volatility of lead oxide during firing with a fast heating rate (upto 580°C/min).

*** Donated by Coors Ceramic Company, 600 9th St., Golden, CO, 80401.

3.3 Characterization

3.3.1 Bulk Properties

The bulk density of the fired pellets were determined by the Archimedes method with the following equation:

$$\rho_b = \frac{W_D \rho_L}{W_s - W_{ss}} \quad (3.1)$$

where;

- ρ_b = bulk density
- W_b = dry weight of the sample
- ρ_L = density of the liquid
- W_s = saturated weight of the sample
- W_{ss} = saturated and suspended weight of the sample

For the calculation of the percentage of theoretical density, the theoretical density of the composite mixtures were determined by the following equation:

$$\rho_c = \frac{1}{\frac{W_A^f}{\rho_A} + \frac{W_B^f}{\rho_B}} \quad (3.2)$$

where;

- ρ_c : theoretical density of the composite mixtures
- ρ_A, ρ_B : theoretical density of each constituent
- W_A^f, W_B^f : weight fraction of each constituent

A, B : PMN - PT and PGS

The theoretical densities of PMN - PT and PGS used in the calculations are 8.11 g/cm^3 and 7.3 g/cm^3 , respectively. The density data reported in the thesis are the average of 2-3 samples for each compositions and firing conditions. Based on these measurements, the standard error for the percent theoretical density data was less than $\pm 0.5\%$.

3.3.2 X-Ray Diffraction(XRD)

XRD was used to identify the phases of all starting materials and calcined powders, and selected fired pellet and thick film samples. A Rigaku Rotaflex anode x-ray diffractometer interfaced with an IBM desk-top computer to process the data was used. The samples were scanned from $10 - 60^\circ$ with a scan rate of $0.05^\circ/\text{sec}$. The XRD procedure used was as follows;

- i) The sample was mounted on a glass slide with double sided tape.
- ii) The glass slide was mounted into the x-ray chamber.
- iii) The scanning conditions were programmed into the computer.

iv) The data was collected by the computer.

3.3.3 Scanning Electron Microscopy with Energy Dispersive Spectroscopy (SEM-EDS)

A JOEL JXA-840 SEM equipped with an energy dispersive x-ray spectroscopy detector (EDS) was used to investigate the microstructural development of bulk and thick film samples. SEM was also used to measure the average particle size of the powders. The samples were coated with either gold or carbon by sputtering. EDS was used for chemical analysis of the grain boundary in bulk samples and on the surface of thick film samples.

3.4 Dielectric Measurements

To decrease the surface effect from lead volatilization, the bulk samples were first ground with 500 grid sand paper. Samples for dielectric measurement were electroded by sputtering gold electrodes, and applying air-dried silver paint to protect the gold electrode and improve electrical contact. Prior to electroding, the dimensions of the samples were measured for the dielectric constant calculation.

The capacitance and dissipation factor were measured from -55 to 125°C with a Hewlett-Packard Precision LCR meter (HP 4284A) and temperature control box. This system was

computer automated with the Lab Windows program. The capacitance and dissipation factor were measured at five frequencies, 0.1, 1, 10, 100 and 1000 KHz. Based on measurements on four samples of a selected composition (PMN - PT) and firing conditions (900°C for 6 hours), the standard error for the dielectric constant values was less than $\pm 5\%$. The resistivity of thick film samples was measured by applying 100V DC at room temperature using a Radiant Technologies.

CHAPTER 4

RESULT AND DISCUSSION

This chapter is divided into two sections. The first section presents the densification behavior, XRD analysis, and microstructural and dielectric property characteristics of bulk samples of PMN - PT with PGS additions. The second section covers the physical and electrical properties of these compositions prepared in thick film form.

4.1 Bulk Samples

4.1.1 Density

Figures 4.1 and 4.2 show the particle size distributions of the starting PMN - PT and PGS powders after two types of milling conditions. The powders shown in Figure 4.1 were ball milled in distilled water with 15 zirconia cylindrical media(10mm x 10mm) for 12 hours, while the powders in Figure 4.2 were milled with 50 zirconia cylinders for 24 hours. In both cases, 50 grams of powder were milled with 100 ml of water in 125 ml nalgene plastic bottles. These two milling conditions resulted in very

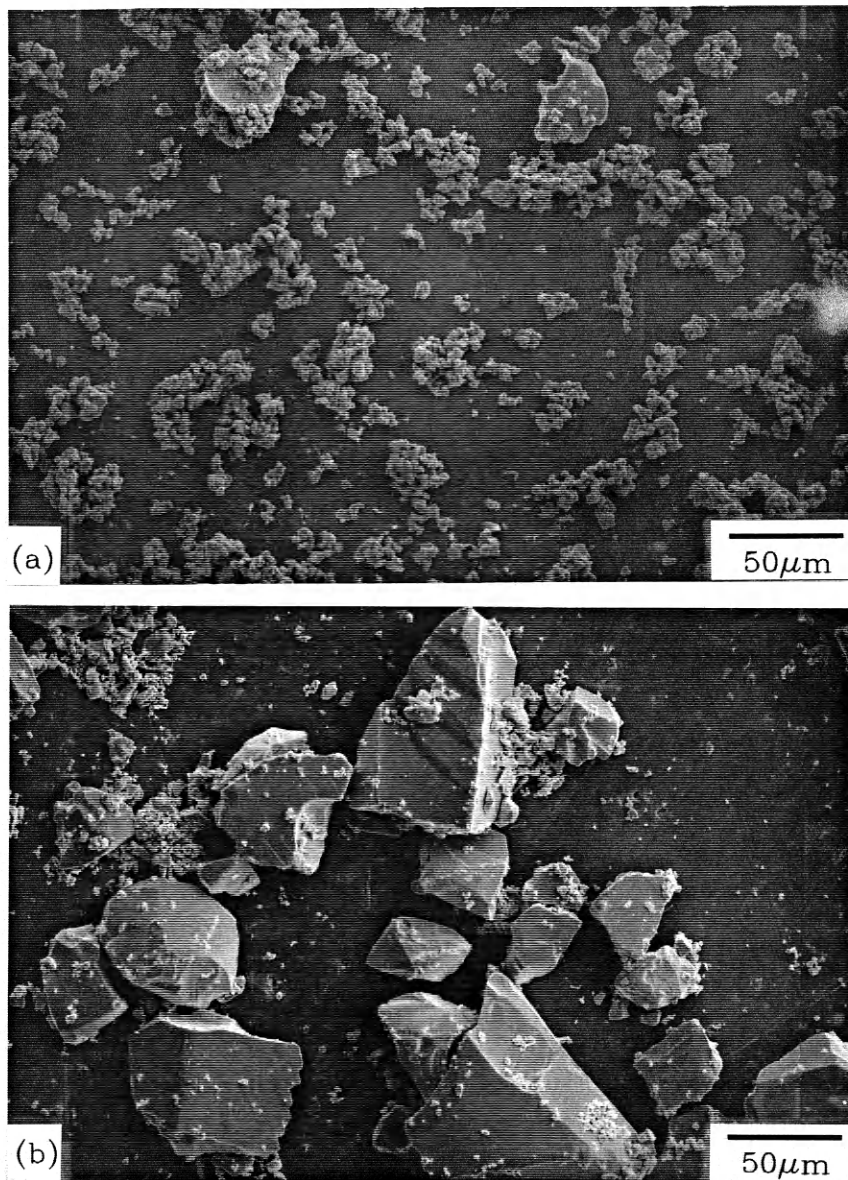


Figure 4.1 SEM micrographs of the a) PMN - PT and b) PGS starting powders, ball milled in distilled water for 12 hours with 15 zirconia cylinders.

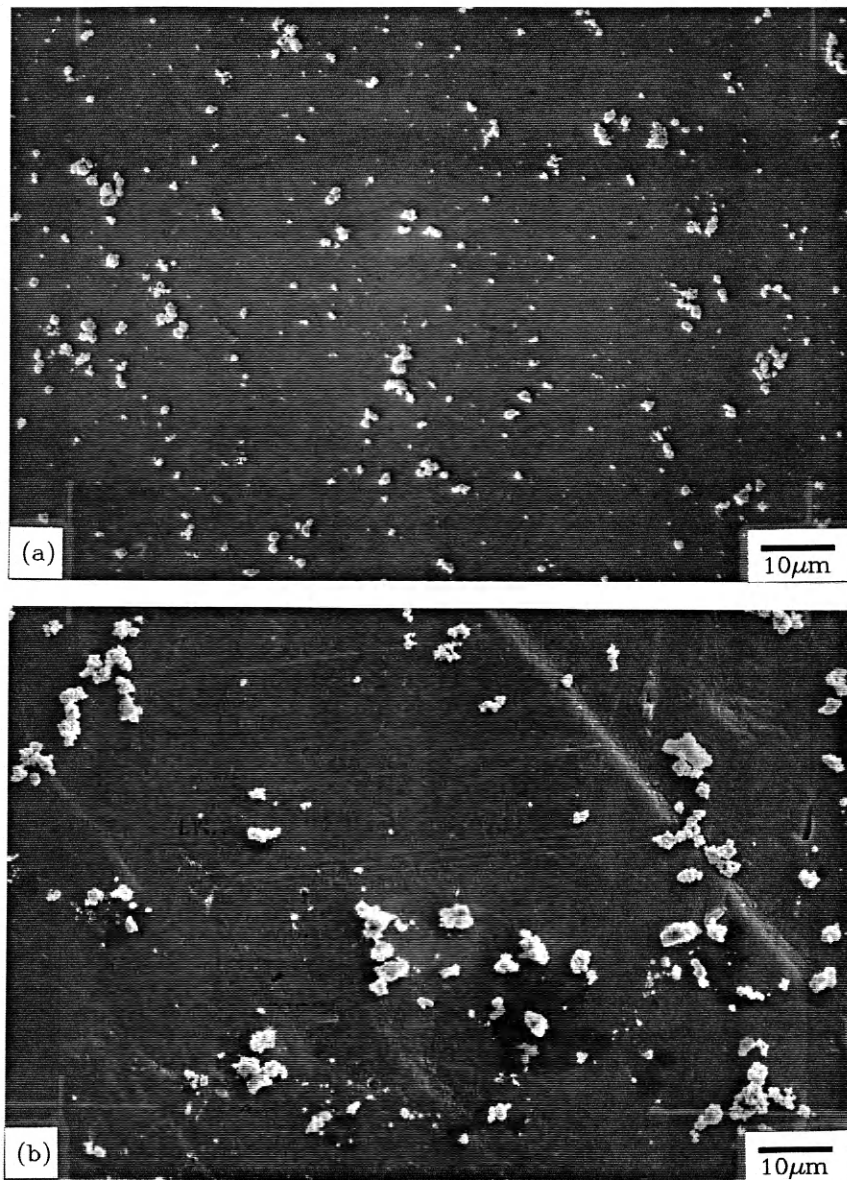


Figure 4.2 SEM micrographs of the a) PMN - PT and b) PGS starting powders, ball milled in distilled water for 24 hours with 50 zirconia cylinders.

different particle size distributions, especially for the PGS glass. The powders which were ball milled with 50 zirconia cylinders for 24 hours had a fine particle size from submicron to several micron. However, the powders which were ball milled with 15 zirconia cylinders for 12 hours had a coarse particle size distribution ranging up to 100 micron in the PGS powder.

Figure 4.3 shows the difference in the percent theoretical density plotted as a function of PGS addition for bulk samples from the powders ball milled by the two different milling conditions discussed above. The samples prepared from the fine powders resulted in greater than 95 percent of the theoretical density. However, the samples from the coarse powders had only 80 - 92 percent of the theoretical density. These results indicate that the reduction in particle size has a significant effect on increasing the density. The samples from the coarse powders show a rapid decrease in density with PGS additions. This appears to be due to the large particles of lead germanium silicate which melted and left large pores during firing. The results presented in the rest of the thesis are for samples prepared from the fine particle sized powders.

Figure 4.4 illustrates the effect of PGS additions on densification of PMN - PT materials fired at 850 and 900°C.

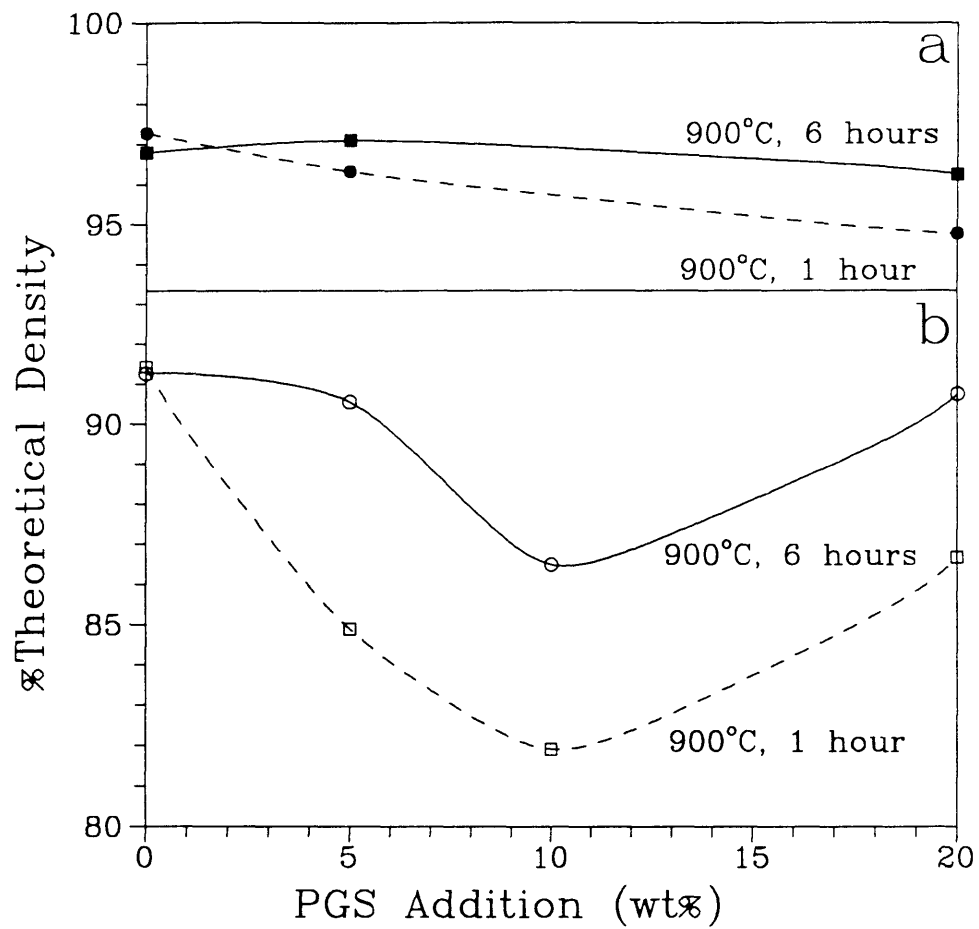


Figure 4.3 The percent theoretical density of pellets from the powders ball milled in distilled water a) for 24 hours with 50 zirconia cylinders and b) for 12 hours with 15 zirconia cylinders plotted versus PGS additions.

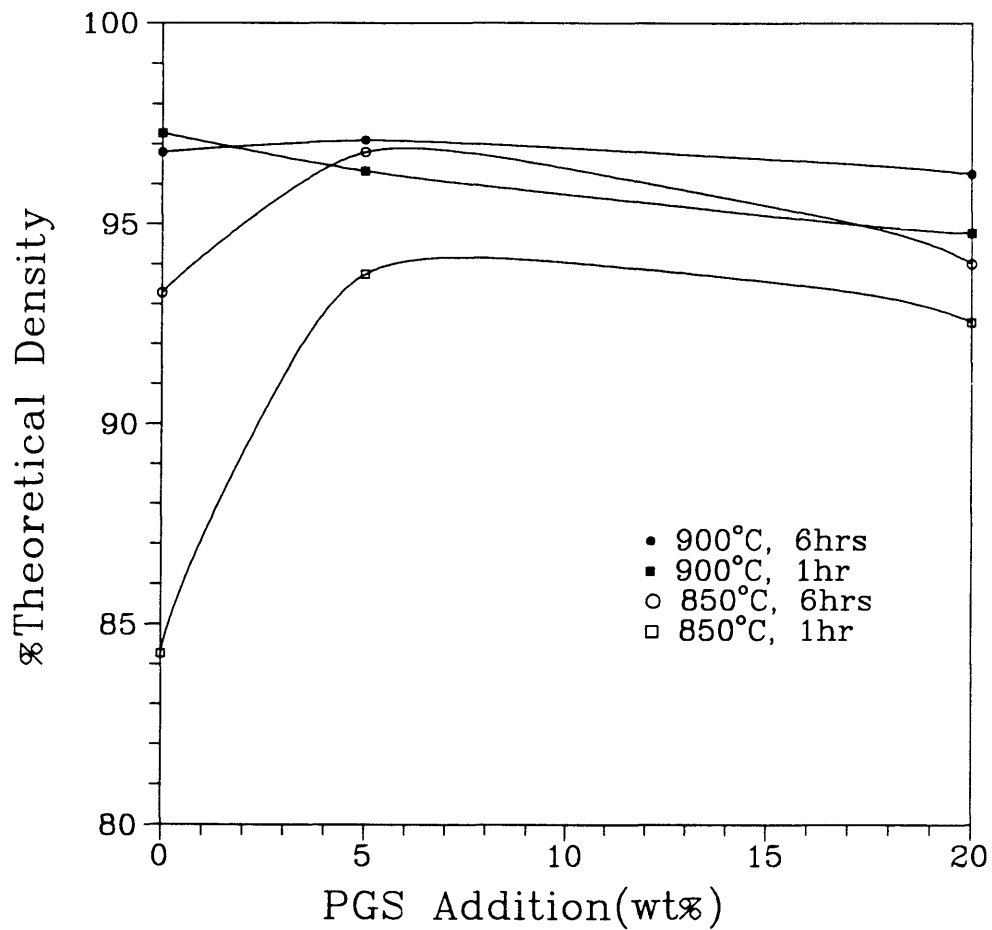


Figure 4.4 The percent theoretical density of pellets fired at 850 and 900°C for 1 and 6 hours plotted versus PGS additions.

The PGS additions do not have a significant effect on the densification of the PMN - PT samples fired at 900°C. However, the density of samples fired at 850°C was significantly increased by the PGS additions. This is due to the liquid phase sintering with PGS addition. More than 5% PGS addition slightly decreased the density of the PMN - PT samples.

The effect of firing temperature and time on the densification of the samples is shown in Figures 4.5 and 4.6. There is no significant difference between the samples prepared with Pb_3O_4 and PbO . The densities of the samples, with and without PGS additions, increase with increasing firing temperature and time. Greater densities were achieved in the PMN - PT samples without PGS additions firing at 900°C compared to 1200°C. Figure 4.6 illustrates the large increase in the percent theoretical density with PGS additions when firing at 850°C for short times.

4.1.2 X-ray Diffraction(XRD)

Both calcined powders and sintered samples were evaluated by x-ray diffraction. The x-ray diffraction patterns of the calcined 0.93PMN - 0.07PT powder is shown in Figure 4.7. The x-ray diffraction patterns of mortar and pestle ground pellets of PMN - PT fired at 850, 900, and

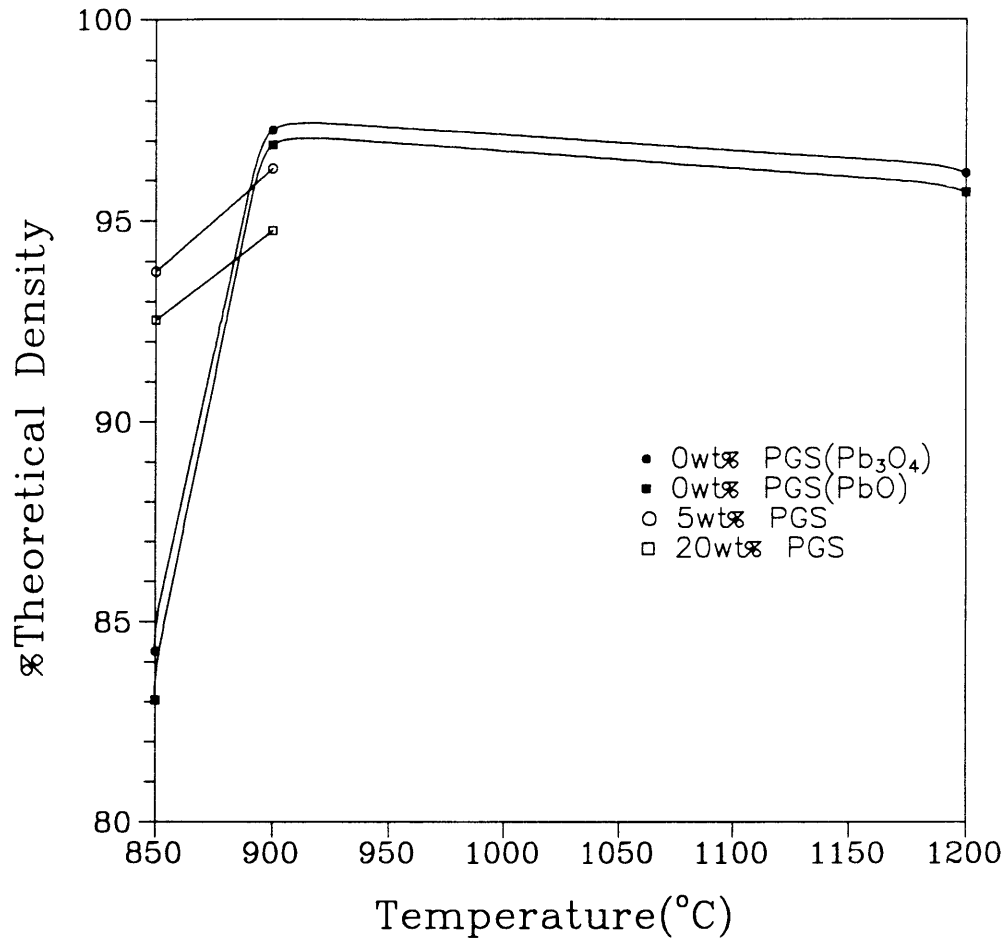


Figure 4.5 The percent theoretical density of PMN - PT pellets with 0, 5, and 20 weight percent PGS additions fired for 1 hour plotted versus temperature.

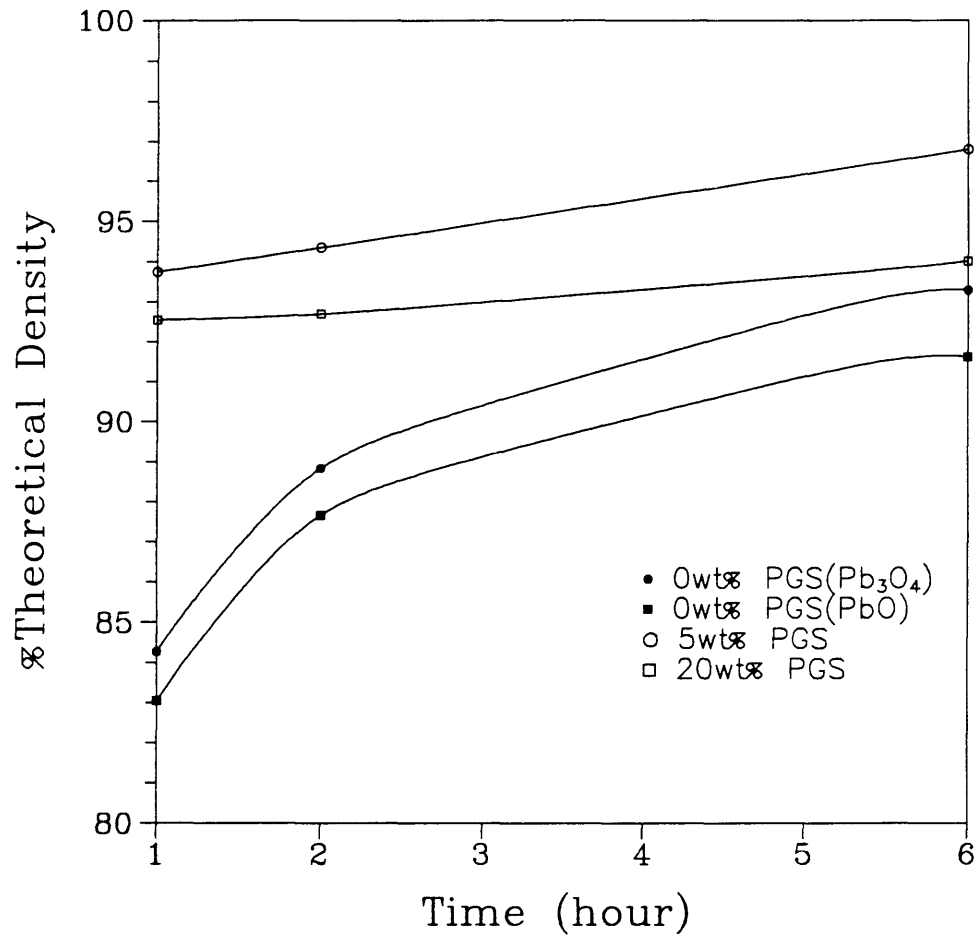


Figure 4.6 The percent theoretical density of PMN - PT pellets with 0, 5, and 20 weight percent PGS additions fired at 850°C plotted versus time.

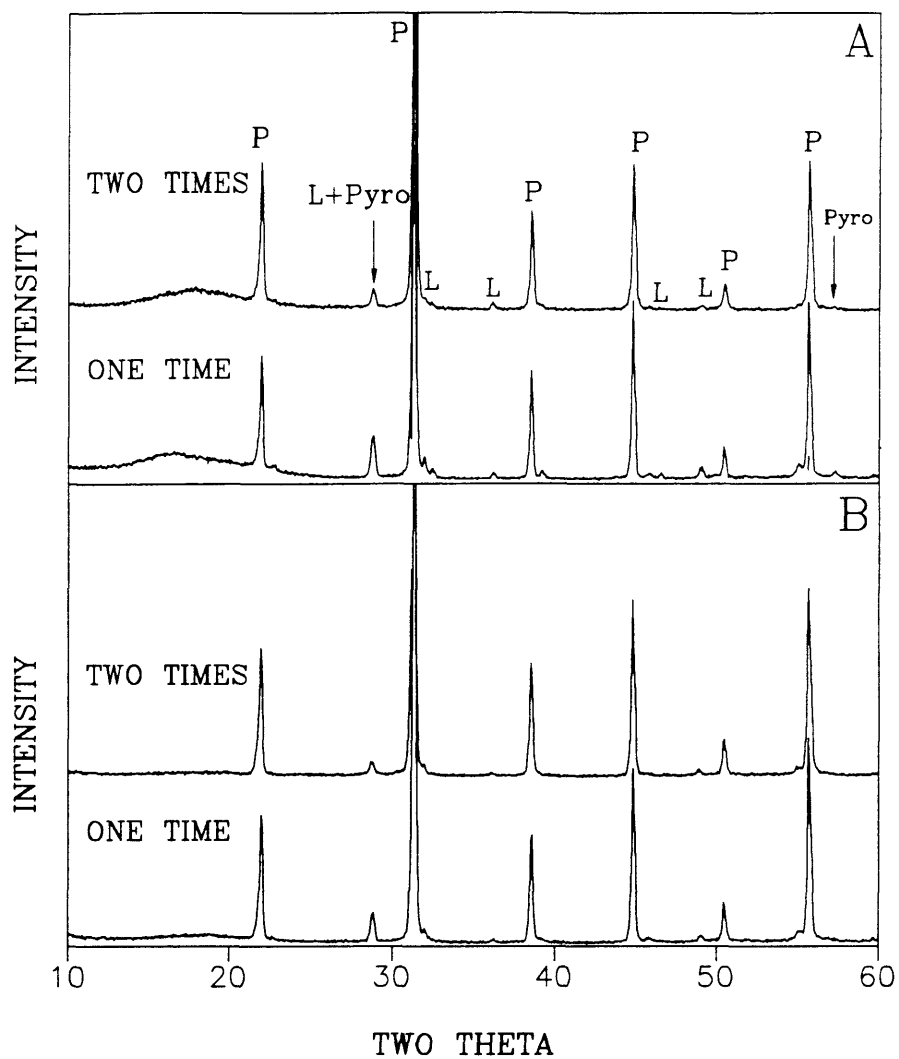


Figure 4.7 X-ray diffraction patterns of PMN - PT powders
 A) prepared from Pb_3O_4 and B) from PbO calcined at $800^\circ C$ for 4 hours one and two times. The peaks in the top pattern are labeled with P for PMN - PT perovskite, L for lead oxide, and Pyro for $Pb_3Nb_2O_8$ pyrochlore.

1200°C for one hour, and 850 and 900°C for six hours are shown in Figures 4.8 to 4.10. Figure 4.7 shows that a small amount of unreacted lead oxide (Pb_3O_4 and PbO) remained in the calcined powders. By repeating the calcination, the unreacted lead oxide was significantly reduced. These phases were not observed in the sintered pellets (see Figures 4.8 to 4.10). A small amount of the pyrochlore ($\text{Pb}_3\text{Nb}_2\text{O}_8$ or $\text{Pb}_3\text{Nb}_4\text{O}_{13}$) phase was observed in the calcined powders and sintered pellets. Repeat calcination or sintering at high temperature reduced the amount of this phase. No significant difference was observed in the x-ray diffraction patterns between the use of Pb_3O_4 compared to PbO .

The amount of pyrochlore phase present in each sample was approximated using the following equation²⁰:

$$\% \text{ Pyro} = \frac{I_{\text{Pyro}}}{I_{\text{Pyro}} + I_{\text{Perov}}} \times 100 \quad (4.1)$$

where, I_{Perov} and I_{Pyro} are the intensities of major x-ray peaks for perovskite (110) and pyrochlore (222) respectively. This equation has been used to provide a simple method of semiquantitatively determining the percentage of pyrochlore.^{25,26,31}

Figures 4.11 and 4.12 show the amount of pyrochlore

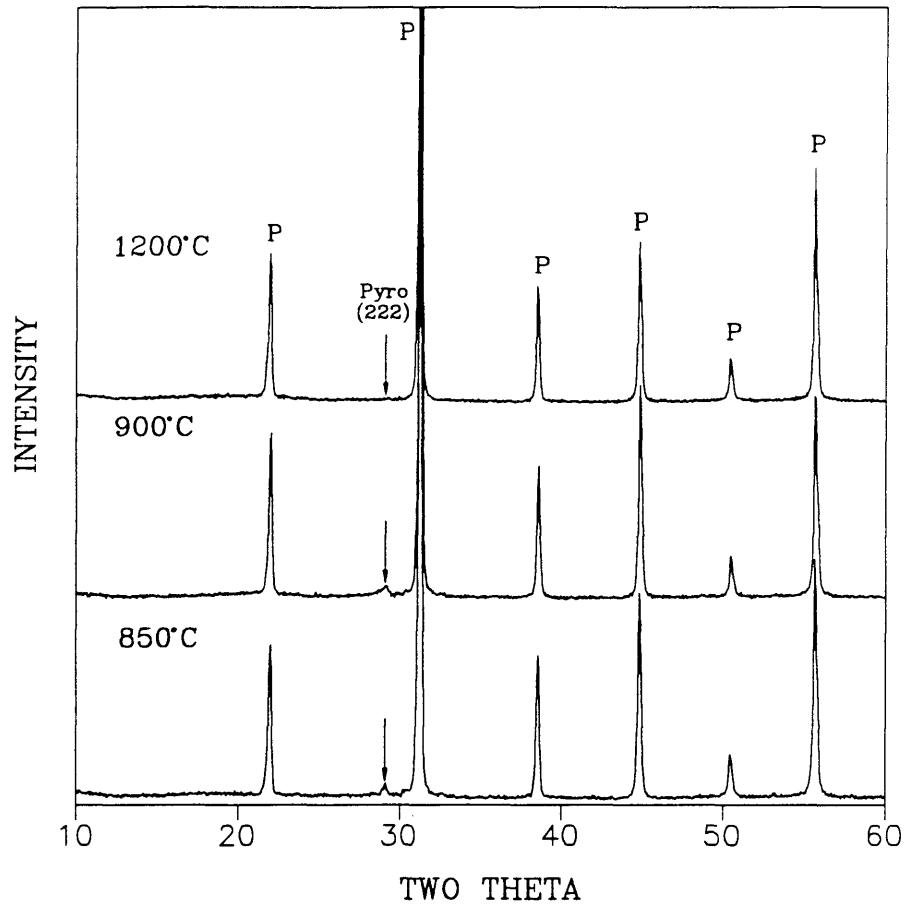


Figure 4.8 X-ray diffraction patterns of PMN - PT samples, prepared from Pb_3O_4 , fired at 850, 900, and 1200°C for 1 hour. The peaks in the top pattern are labeled with P for PMN - PT perovskite and Pyro for $Pb_3Nb_4O_{13}$ pyrochlore.

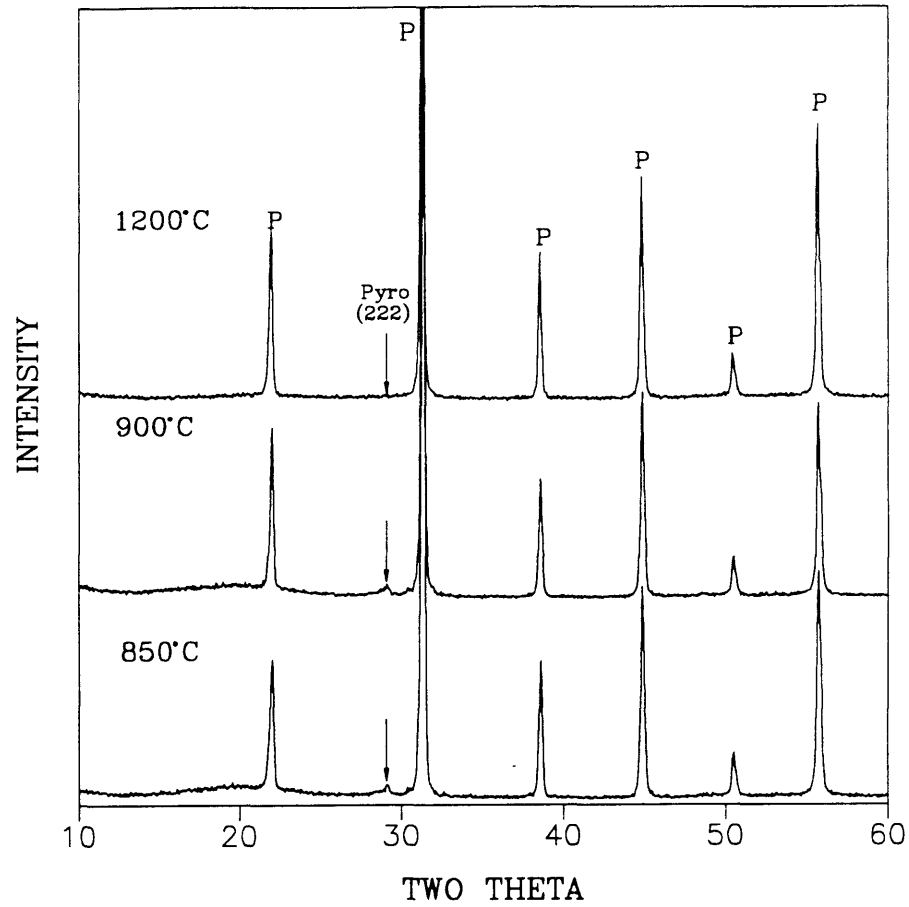


Figure 4.9 X-ray diffraction patterns of PMN - PT samples, prepared from PbO, fired at 850, 900, and 1200°C for 1 hour. The peaks in the top pattern are labeled with P for PMN - PT perovskite and Pyro for Pb₃Nb₄O₁₃ pyrochlore.

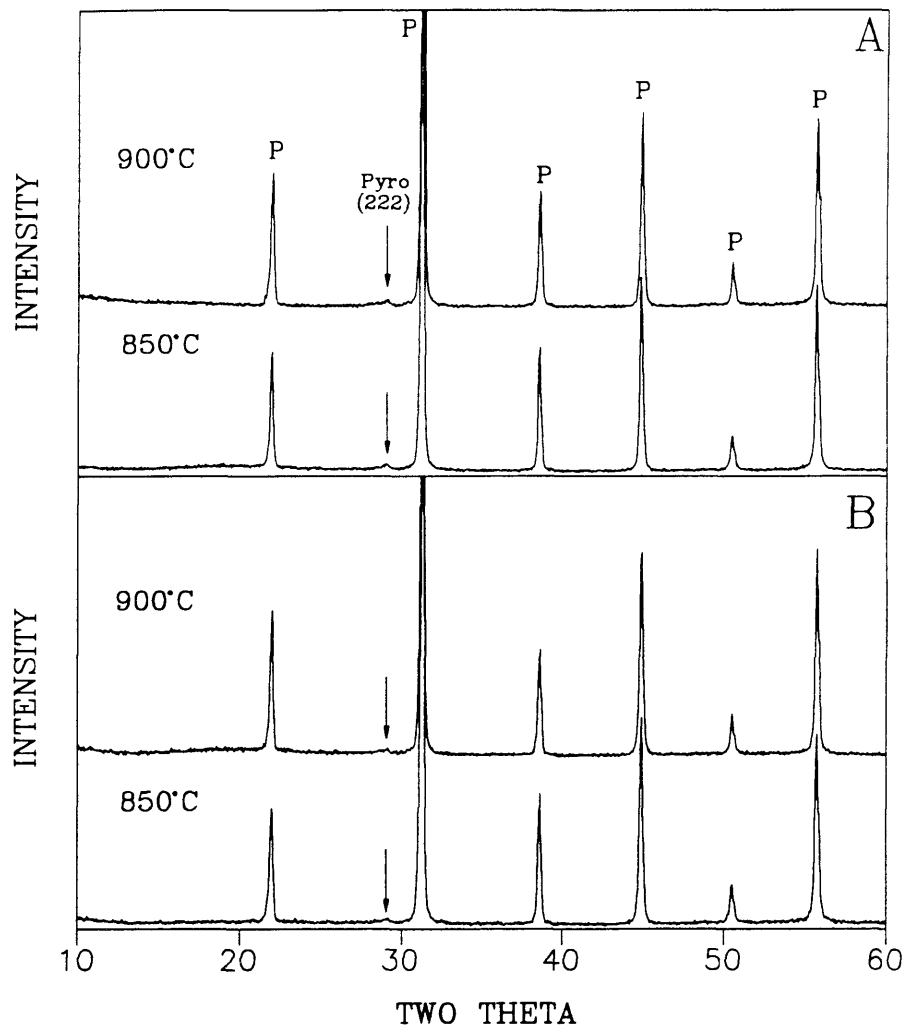


Figure 4.10 X-ray diffraction patterns of PMN - PT samples A) prepared from Pb_3O_4 and B) from PbO fired at 850 and 900°C for 6 hours. The peaks in the top pattern are labeled with P for PMN - PT perovskite and Pyro for $Pb_3Nb_4O_{13}$ pyrochlore.

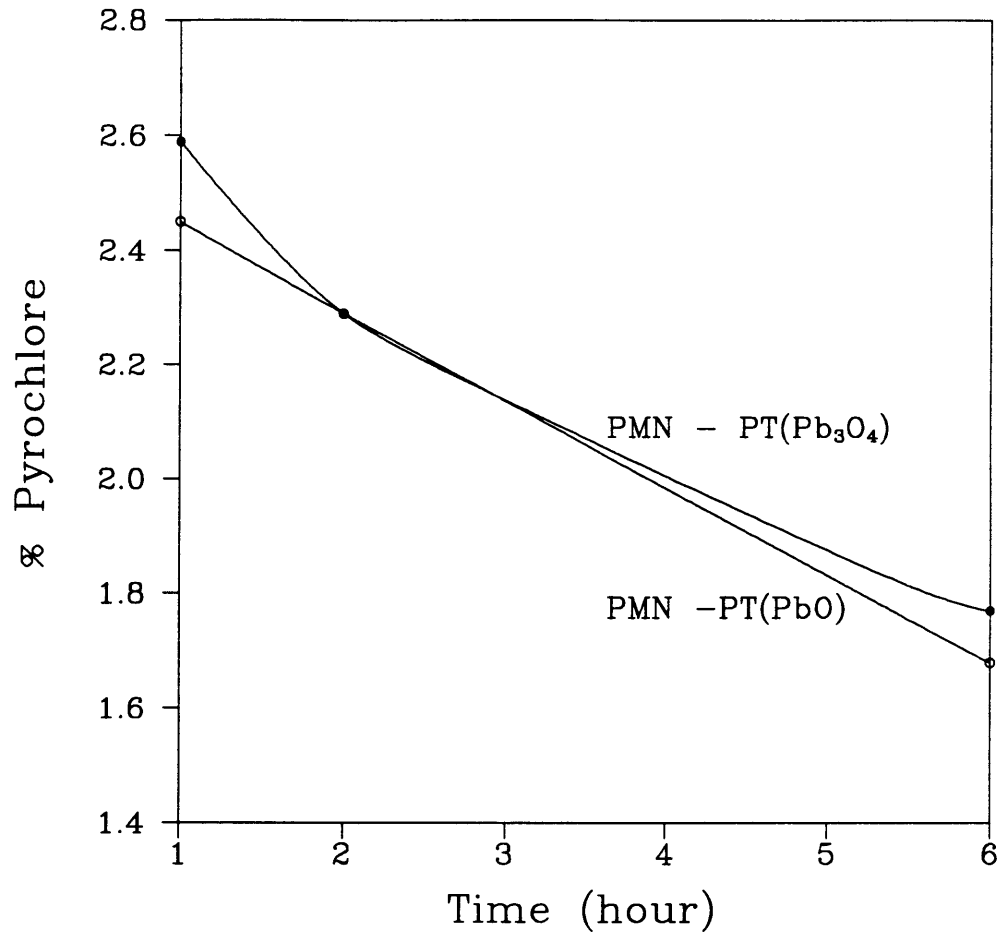


Figure 4.11 The percent pyrochlore phase in pellets fired at 850°C plotted versus time.

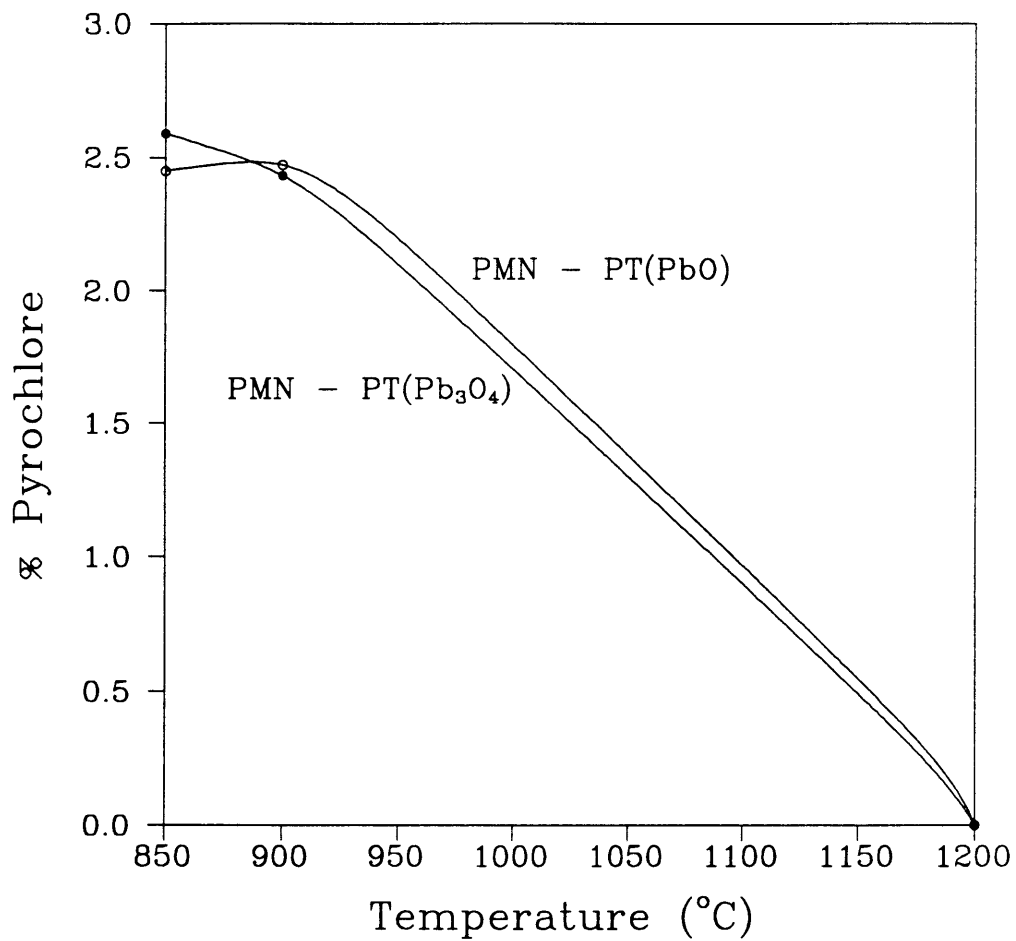


Figure 4.12 The percent pyrochlore phase in pellets fired for 1 hour plotted versus temperature.

phase as a function of time and temperature. As shown in these figures, the samples fired at 850°C for one hour have about 2.5 percent pyrochlore phase, which decreases with increasing sintering time and temperature. The amount of pyrochlore is reduced to an undetectable level at 1200°C.

The pyrochlore phase formed during calcination and sintering. This phase converts into the perovskite PMN - PT with increasing firing temperature and time. However, additional study is needed to more fully understand the formation kinetics, and the effect of lead volatilization.

The x-ray diffraction patterns of a mixture of 80 weight percent PMN - PT and 20 weight percent PGS fired at 900°C for six hours is compared with that of PMN - PT calcined at 800°C for four hours in Figure 4.13. There does not appear to be a significant change in the PMN - PT phase, indicating that the PMN - PT and PGS have not reacted. However, the x-ray diffraction shows that the $Pb_3Ge_{2/3}Si_{1/3}O_5$ phase is formed rather than $Pb_5Ge_2SiO_{11}$. This is possibly due to the removal of lead from the PMN - PT to form the lead rich $Pb_3Ge_{2/3}Si_{1/3}O_5$ phase. This corresponds to the increased formation of the lead deficient pyrochlore phase ($Pb_3Nb_4O_{13}$) as shown in Figure 4.13.

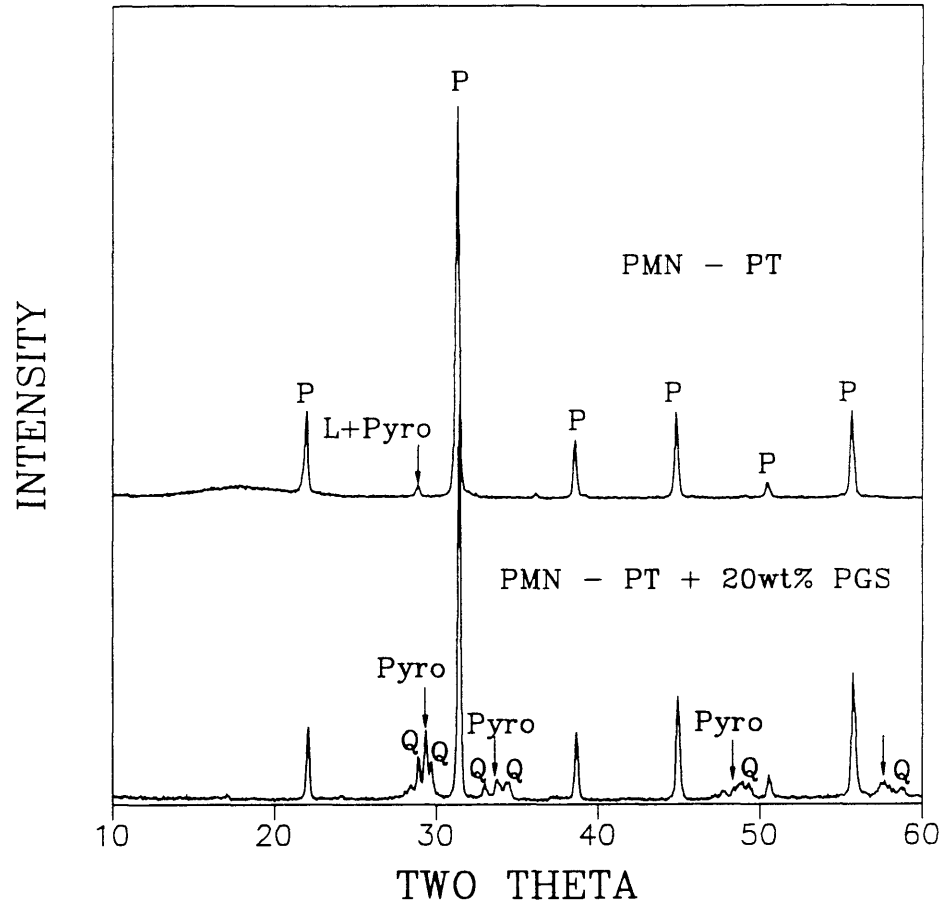


Figure 4.13 X-ray diffraction patterns of calcined (800°C for 4 hours) PMN - PT powder, and PMN - PT with 20wt% PGS addition fired at 900°C for 6 hours. The peaks are labeled with P for PMN - PT perovskite, L for lead oxide, and Q for the $\text{Pb}_3\text{Ge}_{2/3}\text{Si}_{1/3}\text{O}_5$.

4.1.3 Microstructural Analysis

The microstructures of pressed pellets heat-treated at 850 and 900°C for one and six hours are shown in Figures 4.14 to 4.17. These figures show that the grain size of the PMN - PT materials increases with increasing firing temperature and time. However, with the addition of PGS, the firing temperature and time did not significantly affect the grain size. The average grain size of the PMN - PT materials without PGS addition was larger than those with the addition of PGS. The formation of PGS at the grain boundaries appears to prevent the growth of the PMN - PT grains.

A few small cracks were observed inside the PMN - PT samples without PGS addition. The cracks were probably formed during the pressing process, and possibly due to the inhomogeneous stress distribution. Figure 4.18 shows the cross section and surface of a crack formed inside a sample of PMN - PT heat treated at 900°C for 6 hours. A second phase was found to segregate on the surface of the cracks(see Figure 4.18b). Analysis of the chemical composition of the second phase by Energy Dispersive Spectroscopy (EDS), indicated that this second phase is lead oxide.

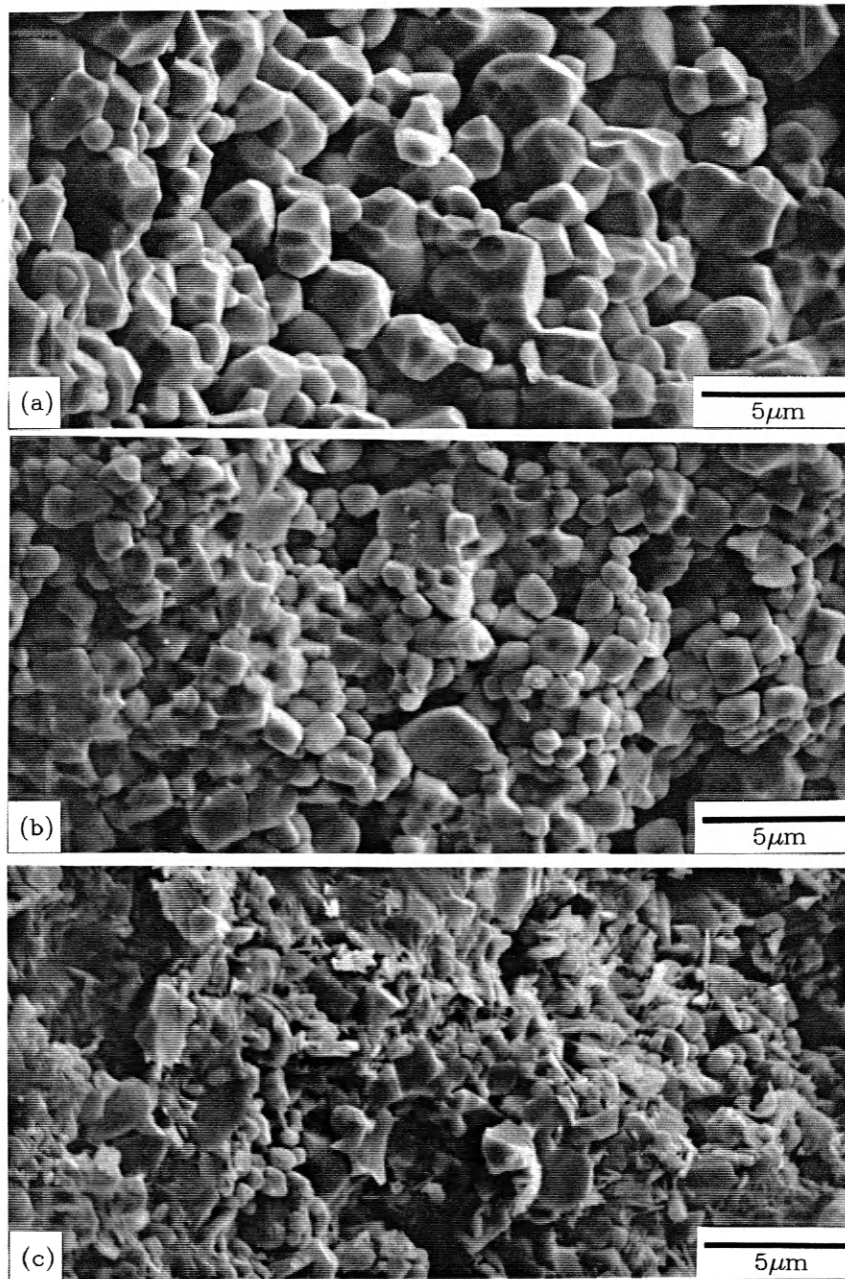


Figure 4.14 SEM micrographs of the fracture surface of pellets fired at 850°C for 1 hour; a) PMN - PT b) PMN - PT with 5wt% PGS addition c) PMN - PT with 20wt% PGS addition.

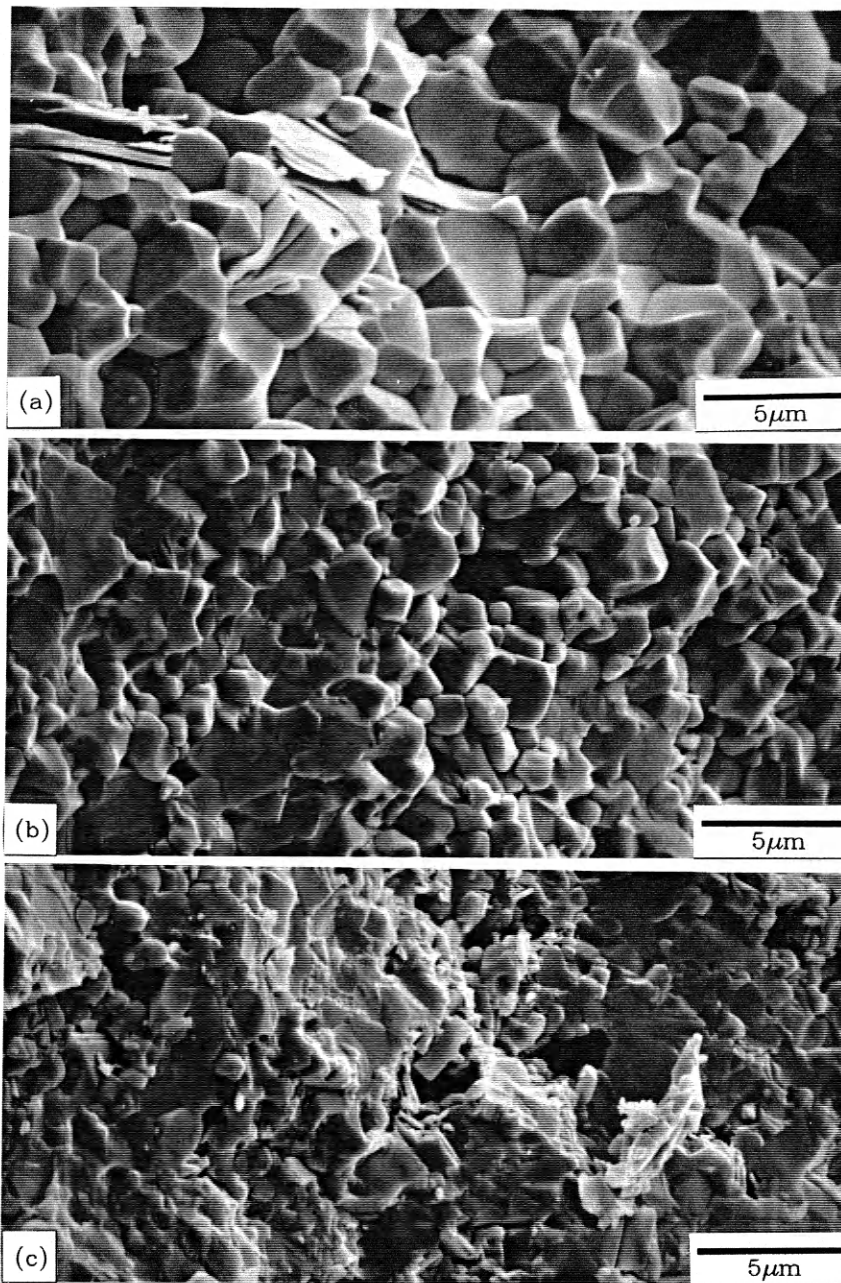


Figure 4.15 SEM micrographs of the fracture surface of pellets fired at 850°C for 6 hours; a) PMN - PT b) PMN - PT with 5wt% PGS addition c) PMN - PT with 20wt% PGS addition.

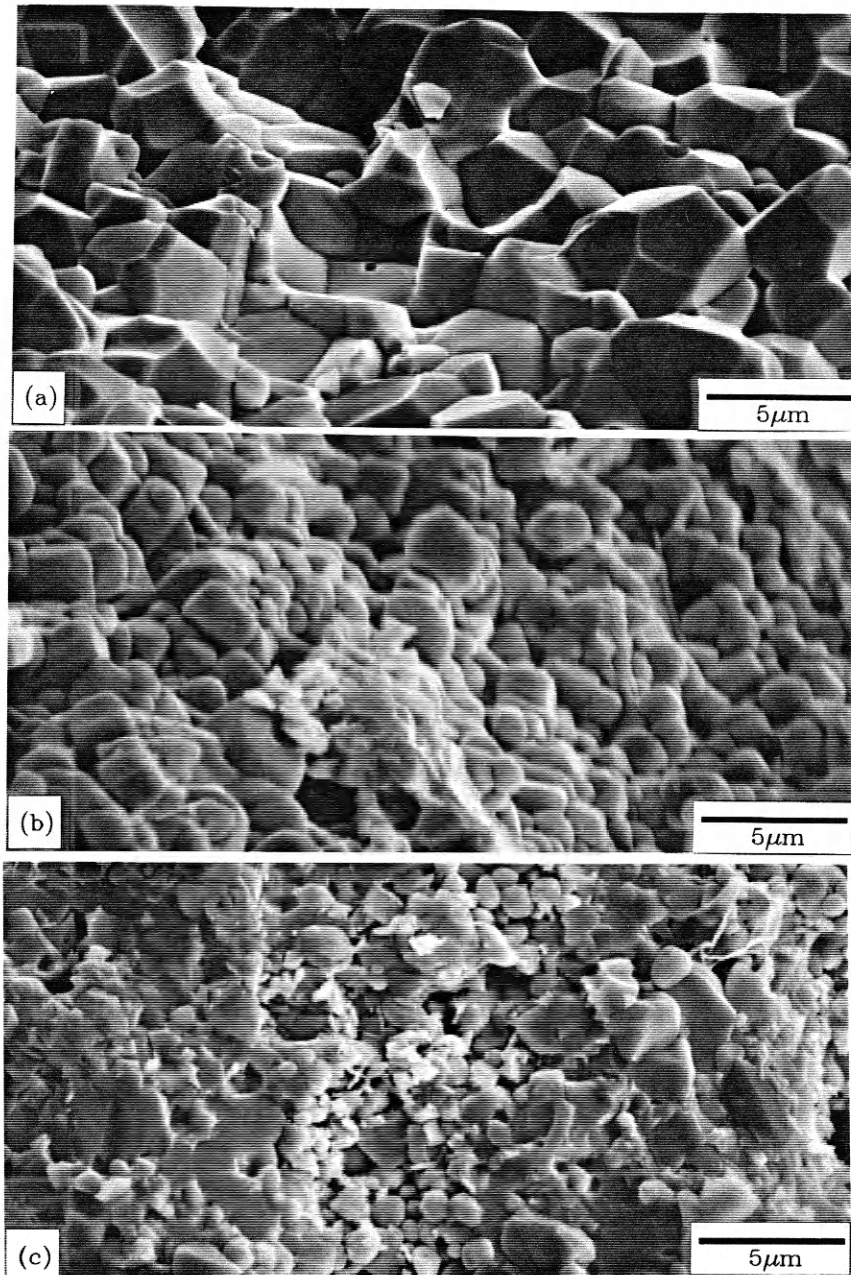


Figure 4.16 SEM micrographs of the fracture surface of pellets fired at 900°C for 1 hour; a) PMN - PT b) PMN - PT with 5wt% PGS addition c) PMN - PT with 20wt% PGS addition.

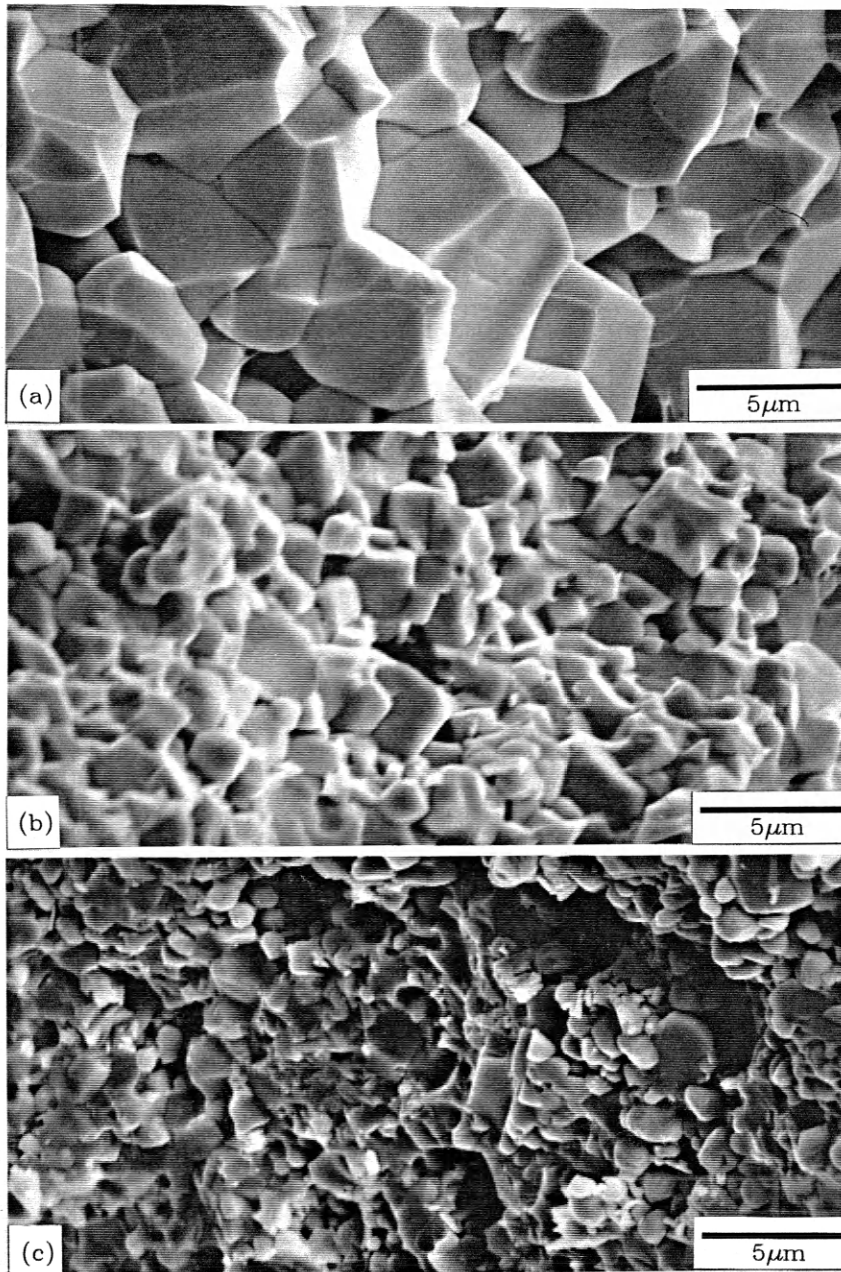


Figure 4.17 SEM micrographs of the fracture surface of pellets fired at 900°C for 6 hours; a) PMN - PT b) PMN - PT with 5wt% PGS addition c) PMN - PT with 20wt% PGS addition.

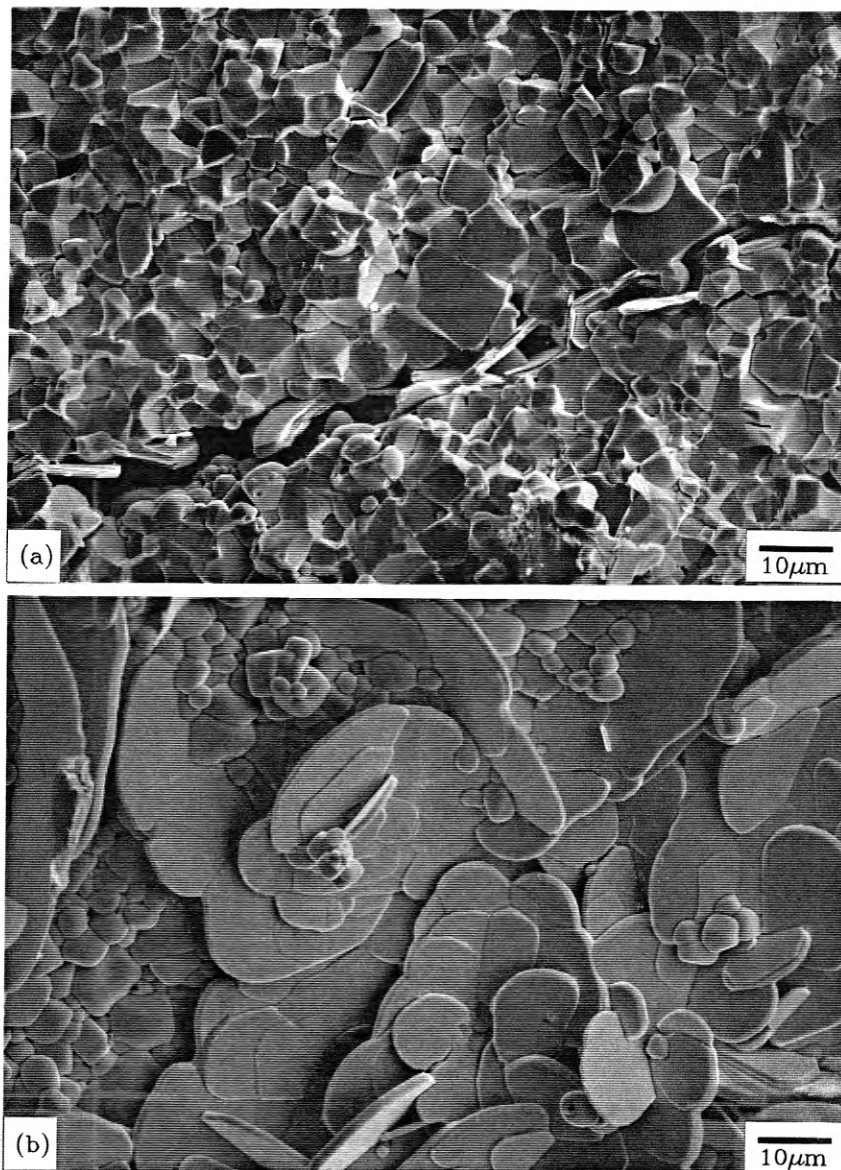


Figure 4.18 SEM micrographs of a crack inside a pellet of PMN - PT fired at 900°C for 6 hours; a) cross - section, and b) surface of the crack.

4.1.4 Dielectric Properties

Figure 4.19 shows the dielectric constant and dissipation factor plotted versus temperature at five low field frequencies for a PMN - PT sample fired at 900°C for six hours. The dielectric constant and dissipation factor show typical relaxor behavior as described in Chapter 2. The transition temperature ($\approx 18^\circ\text{C}$) at 1 KHz is slightly lower than that expected ($\approx 22^\circ\text{C}$) based on the solid solution between PMN and PT.

The temperature dependence of the dielectric constant and dissipation factor for PMN - PT pellets fired at 850 and 900°C for one and six hours is shown in Figure 4.20. Generally, the dielectric constant increases with increasing firing temperature and time, because of grain growth, increased density, and reduction of the low K grain boundary.³² The dissipation factor slightly increased with increasing firing temperature and time.

The dielectric constant and dissipation factor at 1 KHz of samples with and without the addition of PGS heat treated at 900°C for six hours is plotted versus temperature in Figure 4.21. The dielectric constant decreases with increasing PGS addition, because of the formation of a diphasic composite of low dielectric constant PGS ($K \approx 35$ at room temperature) with high dielectric constant PMN - PT

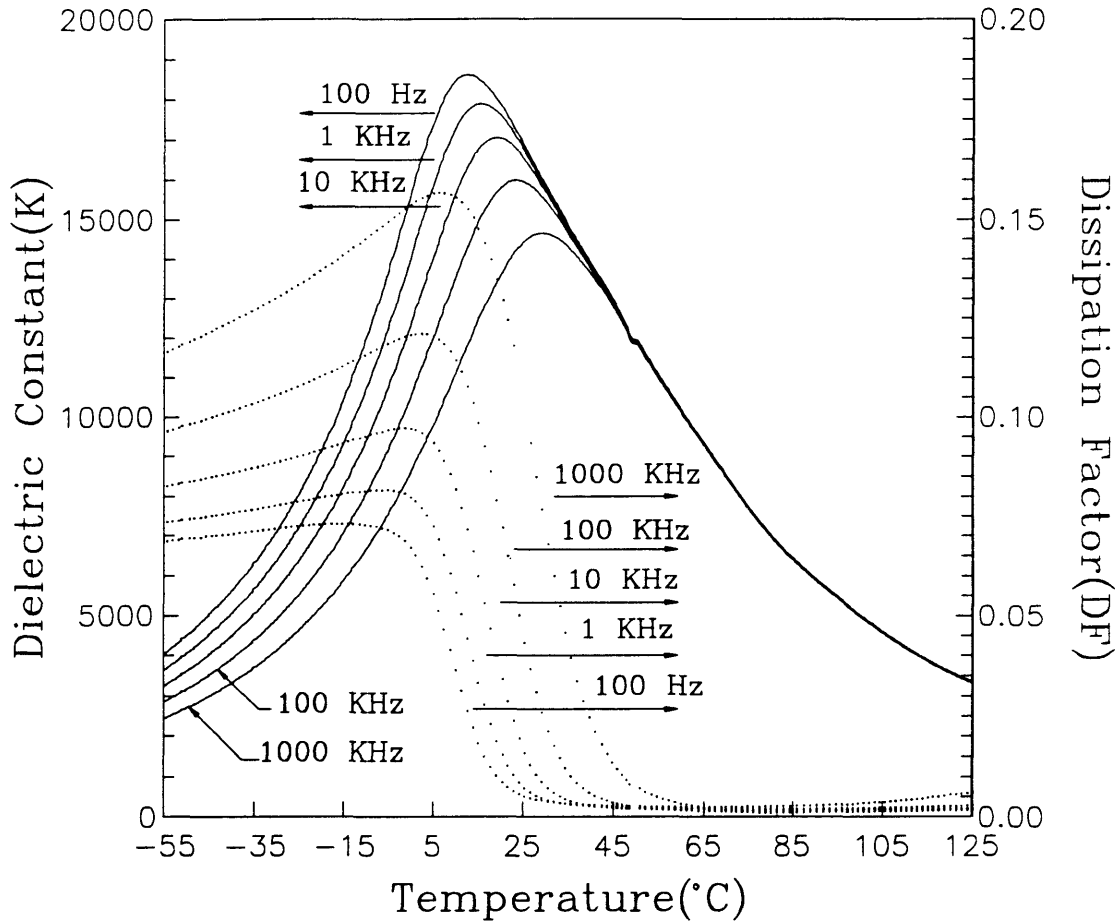


Figure 4.19 The dielectric constant and dissipation factor of a PMN - PT pellet fired at 900°C for 6 hours plotted versus temperature for five frequencies.

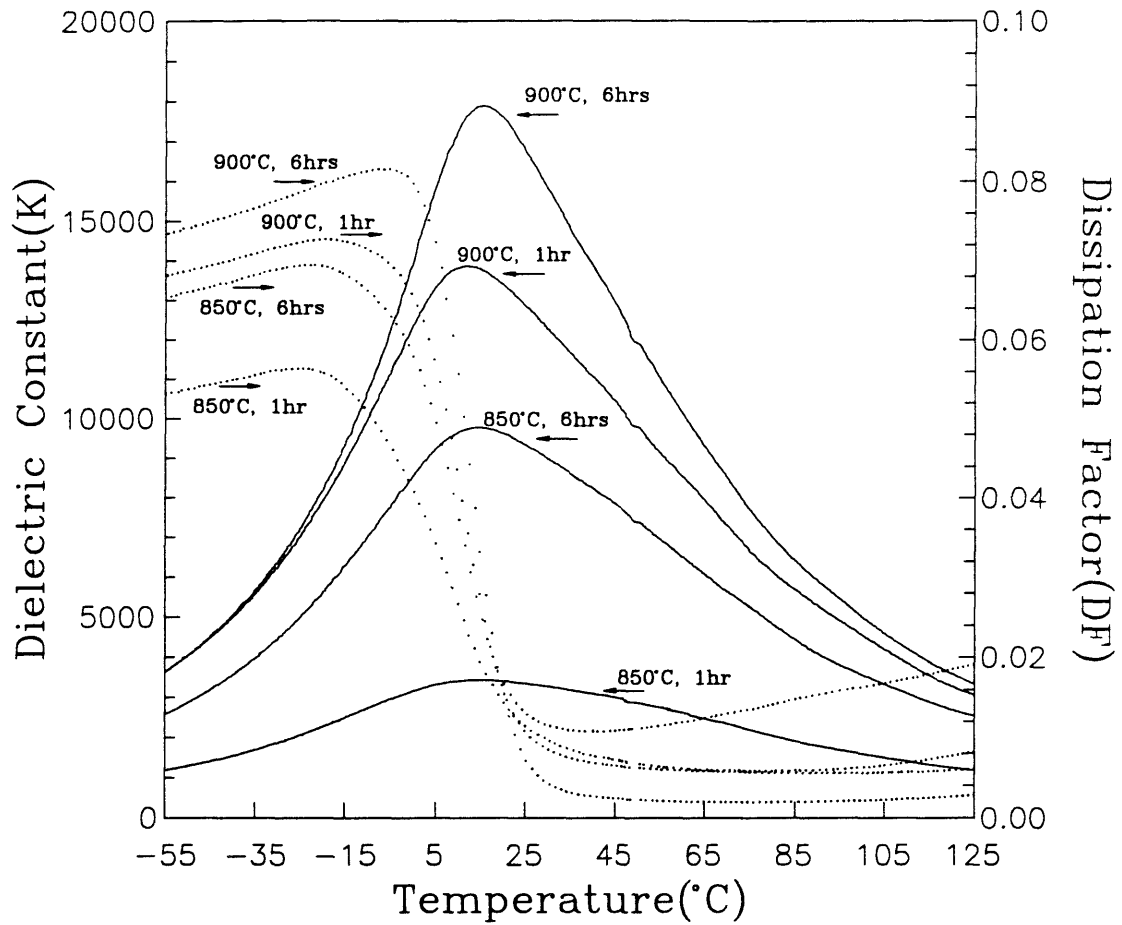


Figure 4.20 Temperature dependence of the dielectric constant and dissipation factor at 1 KHz of PMN - PT pellets fired at 850 and 900°C for 1 and 6 hours.

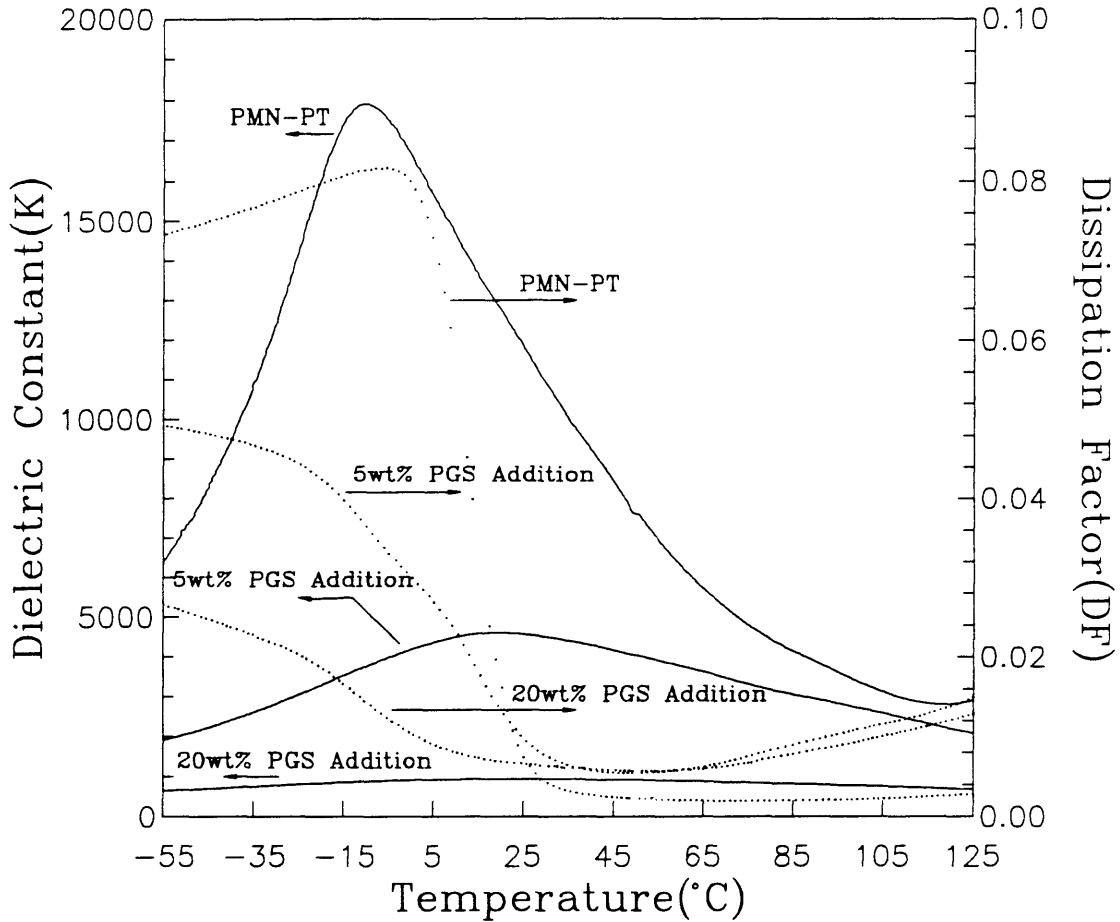


Figure 4.21 Temperature dependence of the dielectric constant and dissipation factor at 1 KHz for PMN - PT with and without PGS additions fired at 900°C for 6 hours.

($K \approx 18,000$ at room temperature). The SEM micrographs shown earlier indicate that the PGS forms a continuous boundary phase between PMN - PT grains. Figure 4.22 shows a comparison of the measured dielectric constant of samples fired at 900°C for six hours with calculated values based on the following series and parallel dielectric mixing rules:

$$\text{Series:} \quad \frac{1}{K_t} = \frac{v_1}{K_1} + \frac{v_2}{K_2}$$

$$\text{Parallel:} \quad K_t = K_1 \cdot v_1 + K_2 \cdot v_2$$

K is dielectric constant and v the volume fraction. Values of 18,000 and 35 were used in the calculation for pure PMN - PT and PGS, respectively. Comparison of the measured and calculated dielectric constants (see Figure 4.22) indicates that the PMN - PT and PGS phases are connected partially in series and partially in parallel. Other factors may have also contributed to the decreased dielectric constant with PGS addition, such as restricted PMN - PT grain growth and the increased formation of the pyrochlore phase (see Section 4.1.2). The effect of PGS addition on the maximum dielectric constant, transition temperature, and density are

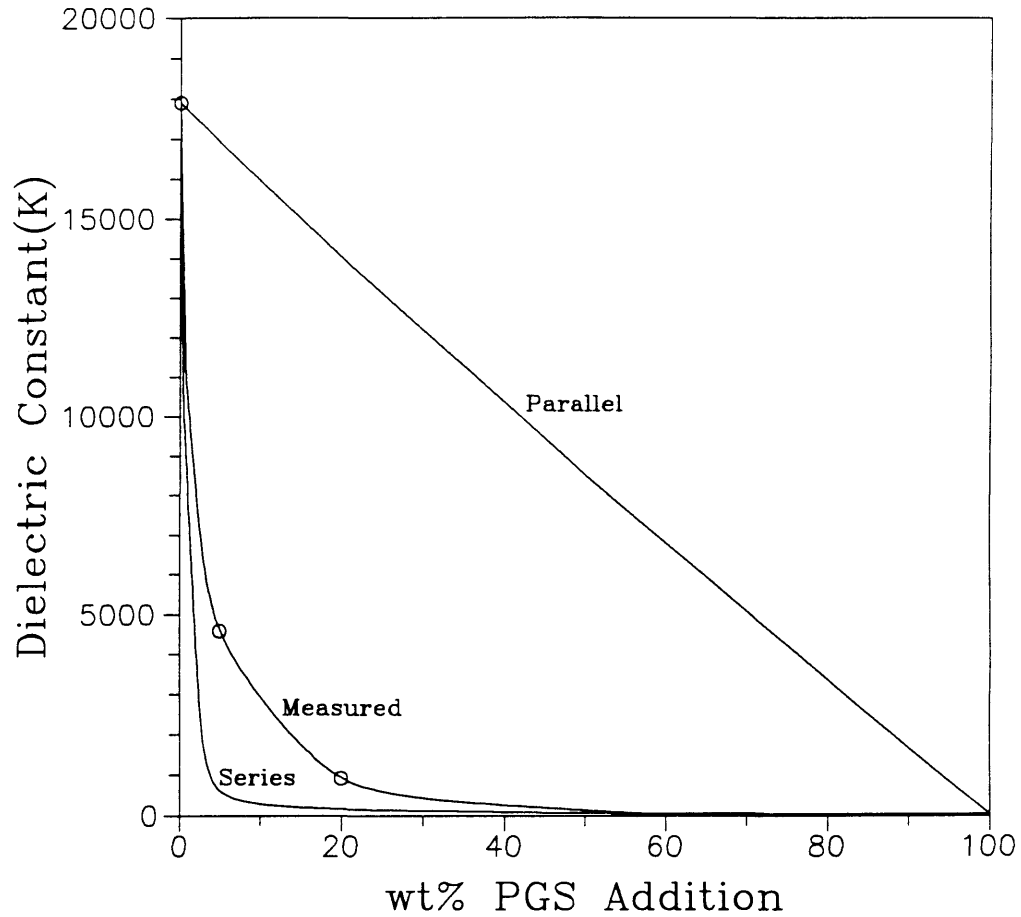


Figure 4.22 The measured dielectric constant of samples fired at 900°C for 6 hours plotted versus PGS addition, compared with calculating based on the series and parallel dielectric mixing models.

summarized in the Table 4.1 for various firing conditions.

Figures 4.23 and 4.24 show the change in capacitance with temperature of samples fired at 850°C for one hour and 900°C for six hours. The temperature coefficient of capacitance (TCC) categories (see Appendix A) of these samples are summarized in the Table 4.2. The PMN - PT without PGS addition has a very large TCC, and belong to the u (+22 to -56%) and v (+22 to -82%) classes. The TCC decreases significantly with increasing PGS addition.

4.1.5 Comparison of Pb_3O_4 and PbO

PMN - PT powders were made with both Pb_3O_4 and PbO. The temperature dependence of the dielectric constant of pellets prepared from these powders, heat treated at 900 and 1200°C for one hour, is shown in Figure 4.25. A comparison of the resulting properties is summarized in Table 4.2. There is no difference in the resulting density and the formation of pyrochlore phases between samples with Pb_3O_4 and PbO.

The difference in the resulting dielectric properties may be due to the difference in the grain size and grain boundary conditions, however additional research is needed to further investigate this. Except where indicated, the data presented in this thesis were collected on samples

Table 4.1 The effect of PGS addition on the dielectric constant, transition temperature, and density of the samples heat treated at 850 and 900°C for 1 and 6 hours.

| | K_{\max} (1 KHz) | | K_{\max} (1 KHz) | |
|-----------|--------------------|---------|--------------------|---------|
| | Fired at 850°C | | Fired at 900°C | |
| | 1 Hour | 6 Hours | 1 Hour | 6 Hours |
| PMN - PT | 3433 | 9780 | 13373 | 17897 |
| 5wt% PGS | 2078 | 2669 | 2351 | 4608 |
| 20wt% PGS | 656 | 806 | 468 | 938 |

| | T_c (1 KHz) | | T_c (1 KHz) | |
|-----------|----------------|---------|----------------|---------|
| | Fired at 850°C | | Fired at 900°C | |
| | 1 Hour | 6 Hours | 1 Hour | 6 Hours |
| PMN - PT | 15.2°C | 14.6°C | 14.9°C | 15.5°C |
| 5wt% PGS | 23°C | 23.6°C | 23.9°C | 18.7°C |
| 20wt% PGS | 12.7°C | 22.9°C | 18.6°C | 23.5°C |

| | Density | | Density | |
|-----------|----------------|---------|----------------|---------|
| | Fired at 850°C | | Fired at 900°C | |
| | 1 Hour | 6 Hours | 1 Hour | 6 Hours |
| PMN - PT | 84.3% | 93.3% | 97.3% | 96.8% |
| 5wt% PGS | 93.7% | 96.8% | 96.3% | 97.1% |
| 20wt% PGS | 92.5% | 94.0% | 94.8% | 96.2% |

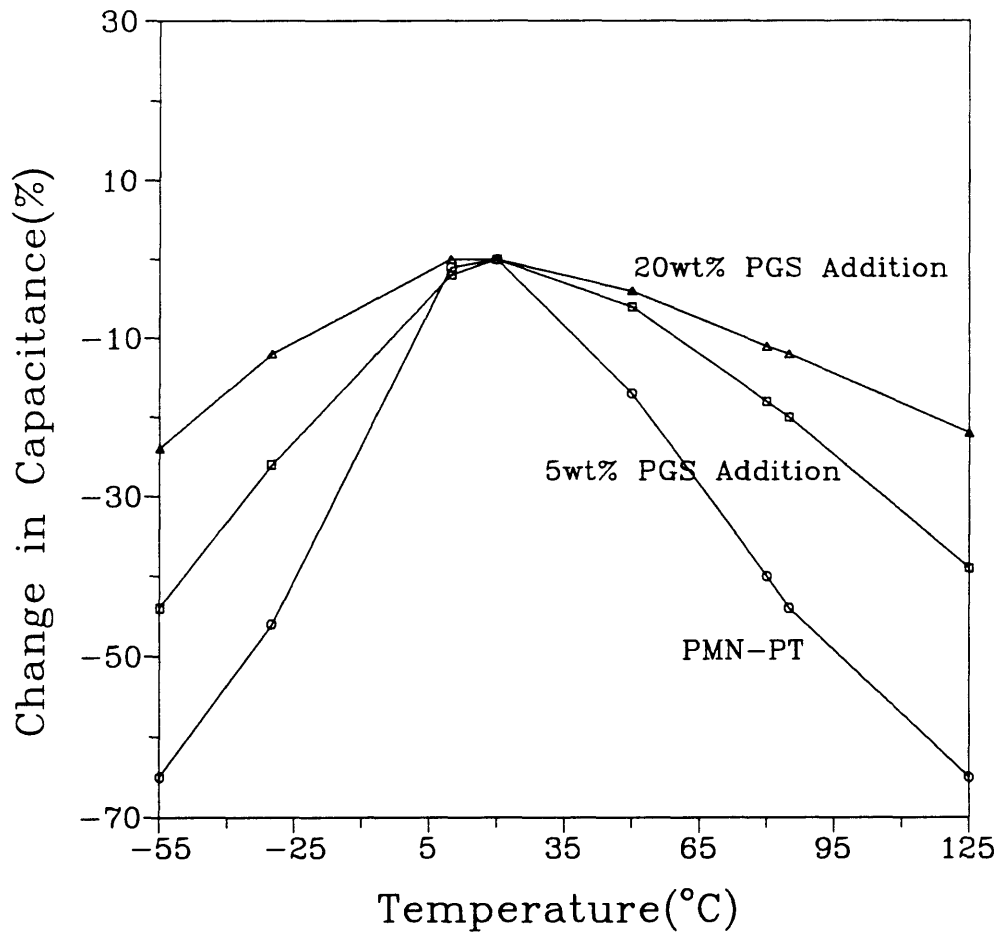


Figure 4.23 Change in capacitance ($\Delta C/C$) of samples fired at 850°C for 1 hour plotted versus temperature.

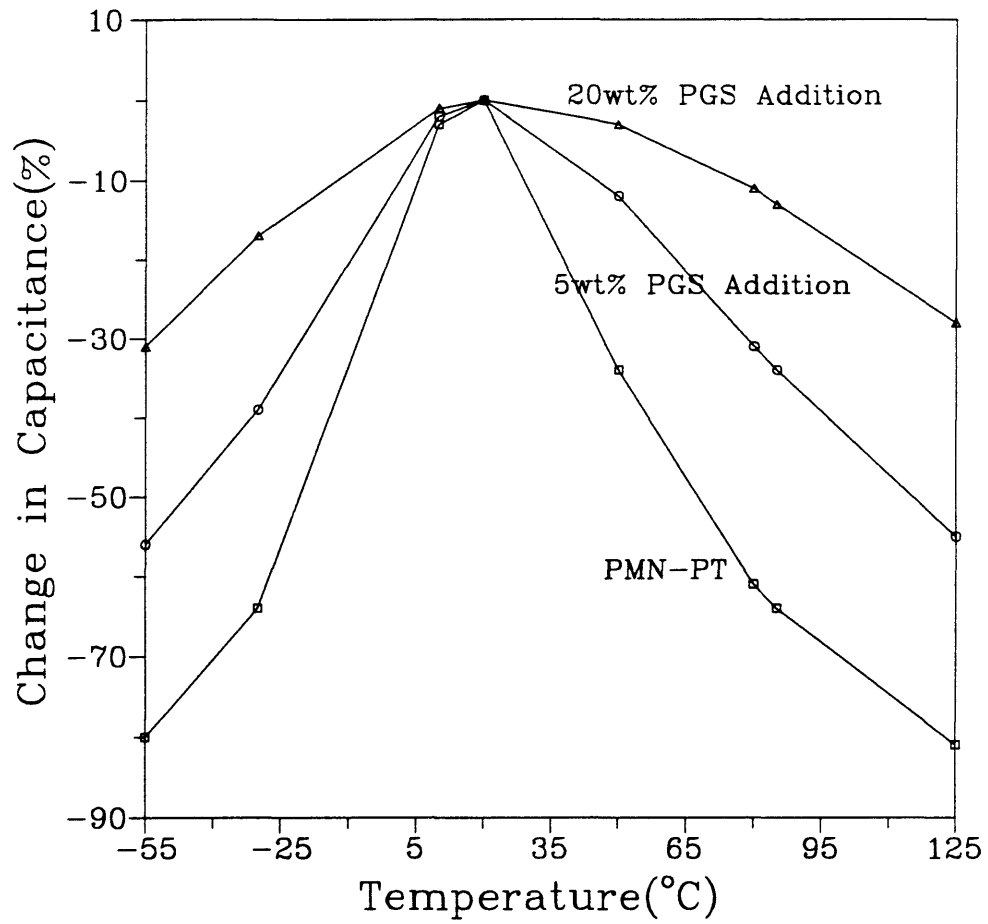


Figure 4.24 Change in capacitance ($\Delta C/C$) of samples fired at 900°C for 6 hours plotted versus temperature.

Table 4.2 The TCC categories of the PMN - PT samples with 0, 5, and 20wt% PGS additions heat treated at 850 and 900°C for 1 and 6 hours.

| | | TCC* | | | |
|-----------|-------------------|------|-----|-----|-----|
| | | X7 | X5 | Y5 | Z5 |
| PMN - PT | 850°C, 1 Hour | X7V | X5V | Y5U | Z5V |
| | 900°C, 6 Hours | X7V | X5V | Y5V | Z5V |
| 5wt% PGS | 850°C, 1 Hour | X7U | X5U | Y5T | Z5S |
| | 900°C, 6 Hours | X7U | X5U | Y5U | Z5T |
| 20wt% PGS | 850°C, 1 Hour | X7T | X5T | Y5R | Z5R |
| | 900°C, 6 Hours | X7T | X5T | Y5S | Z5R |

* See Appendix A

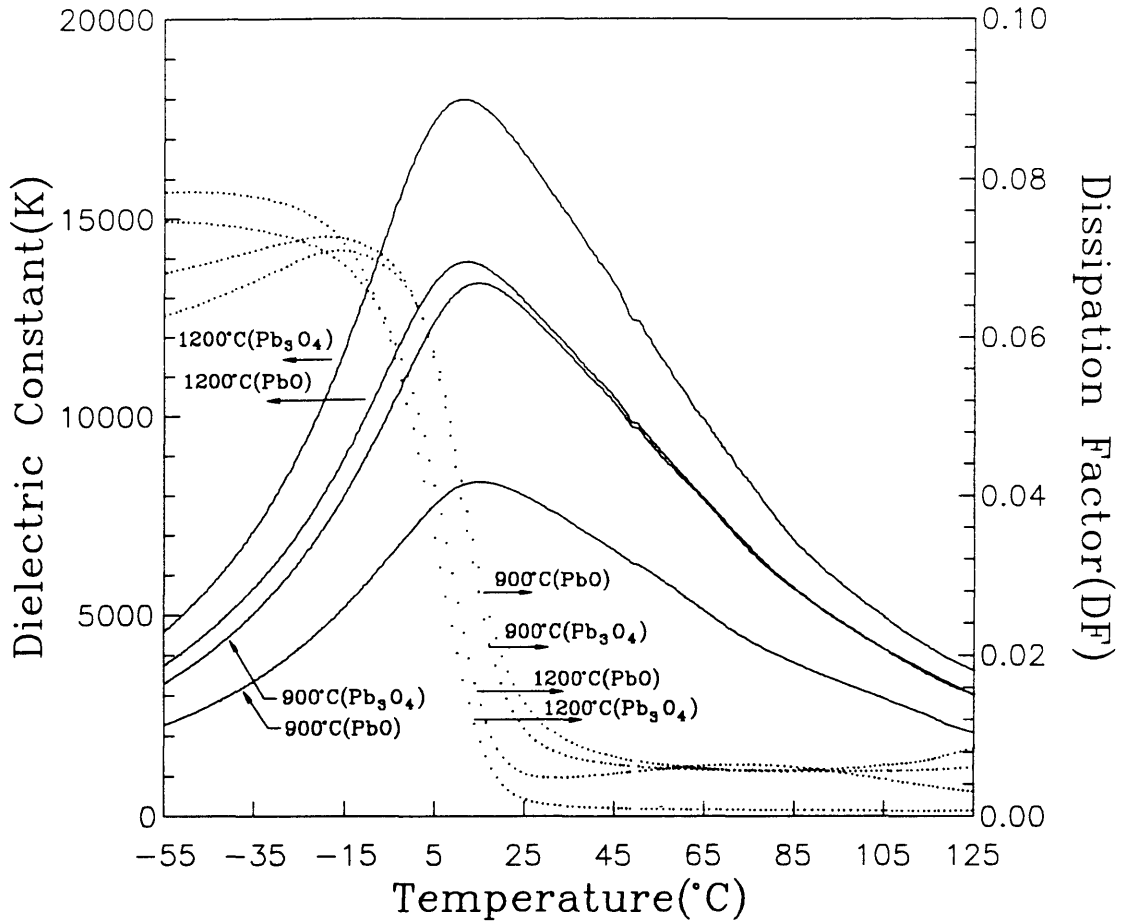


Figure 4.25 The temperature dependence of the dielectric constant and dissipation factor of PMN - PT pellets fired at 900 and 1200°C for 1 hour, comparing the use of Pb₃O₄ and PbO raw materials.

Table 4.3 Comparison of the resulting properties of PMN - PT pellets prepared with Pb_3O_4 and PbO raw materials.

| | % Pyrochlore | | K_{max} (1 KHz) | | Density | |
|---|--------------|-------|-------------------|-------|-----------|-------|
| | Pb_3O_4 | PbO | Pb_3O_4 | PbO | Pb_3O_4 | PbO |
| Calcined two times at 800°C for 4 Hours | 0% | 0% | * | * | * | * |
| Fired at 850°C for 1 Hour | 2.59% | 2.45% | 3433 | 4792 | 84.3% | 83.1% |
| Fired at 850°C for 2 Hours | 2.29% | 2.29% | * | * | 88.8% | 87.7% |
| Fired at 850°C for 6 Hours | 1.77% | 1.68% | 9780 | 7331 | 93.3% | 91.6% |
| Fired at 900°C for 1 Hour | 2.43% | 2.47% | 13373 | 8350 | 97.3% | 96.9% |
| Fired at 900°C for 6 Hour | 1.74% | 1.93% | 17897 | 20859 | 96.8% | 96.9% |
| Fired at 1200°C for 1 Hour | 0% | 0% | 17985 | 13912 | 96.2% | 95.7% |

prepared with Pb_3O_4 used as the lead oxide raw material.
This includes both the preparation of the PMN - PT and PGS
powders.

4.2 Thick Film Samples

4.2.1 Density

The data presented in this section were collected on samples heat-treated at 850 and 900°C (typical thick film processing temperatures). The thick film pastes were prepared from the fine particle size PMN - PT powder which was ball milled with 50 zirconia cylinders for 24 hours, and the calcined PGS powder.

Figure 4.26 shows the fractured cross section of thick film PMN - PT with PGS addition samples heat-treated at 850°C for three hours with a heating rate of 3.33°C/min. The PMN - PT in thick film form did not densify at 850°C even with 20 weight percent PGS addition, although the bulk samples did densify to about 95 percent of the theoretical density with 5 weight percent PGS addition. This is because only one directional shrinkage is allowed in thick film form. The substrate hinders the densification of the thick film layers in the parallel directions to the substrate. The samples with 40 weight percent PGS addition did densify to closed porosity at 850°C as shown in Figure 4.26c. Thus, a significantly greater amount of PGS is required to densify PMN - PT at 850°C in thick film form compared to in bulk samples (>20wt% versus 5wt%).

Figure 4.27 shows the fractured cross sections of thick

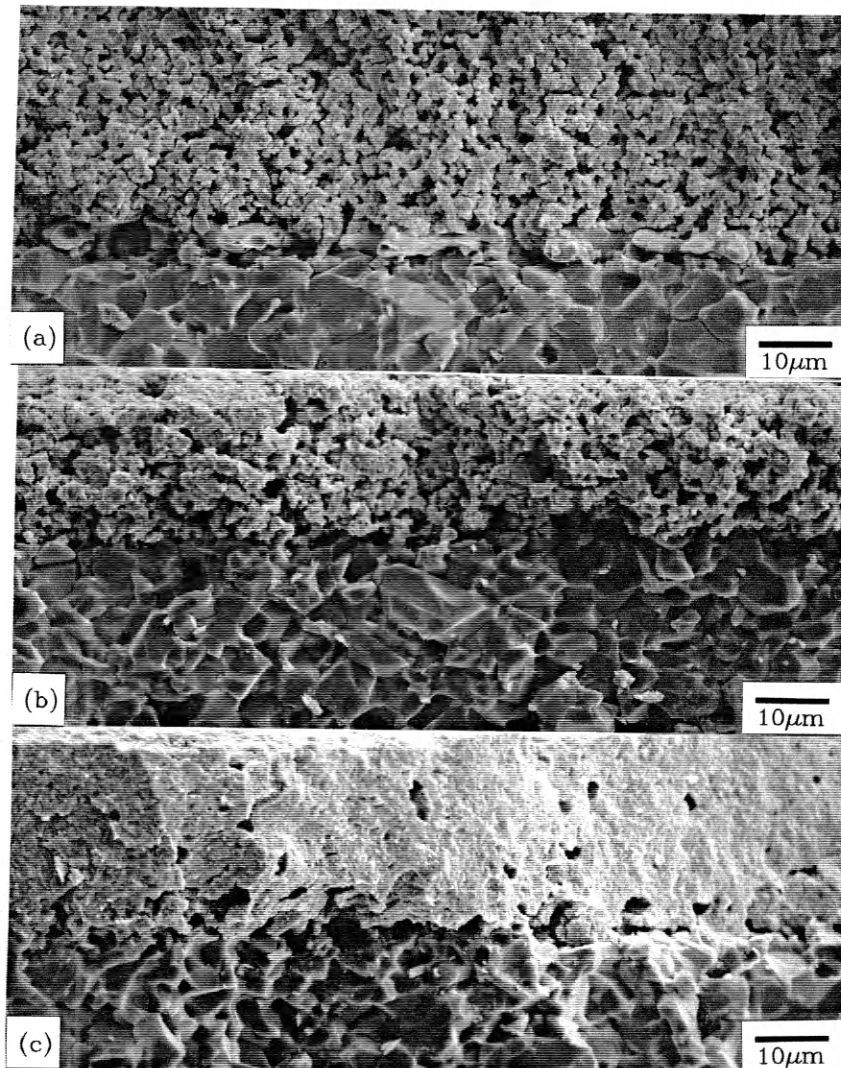


Figure 4.26 SEM micrographs of the fractured cross sections of thick film samples fired at 850°C for 3 hours with a heating rate of 3.33°C/min; a) PMN - PT + 5wt% PGS b) PMN - PT + 20wt% PGS c) PMN - PT + 40wt% PGS. The thick film layers are shown on the top of the photos with the alumina substrate on the bottom.

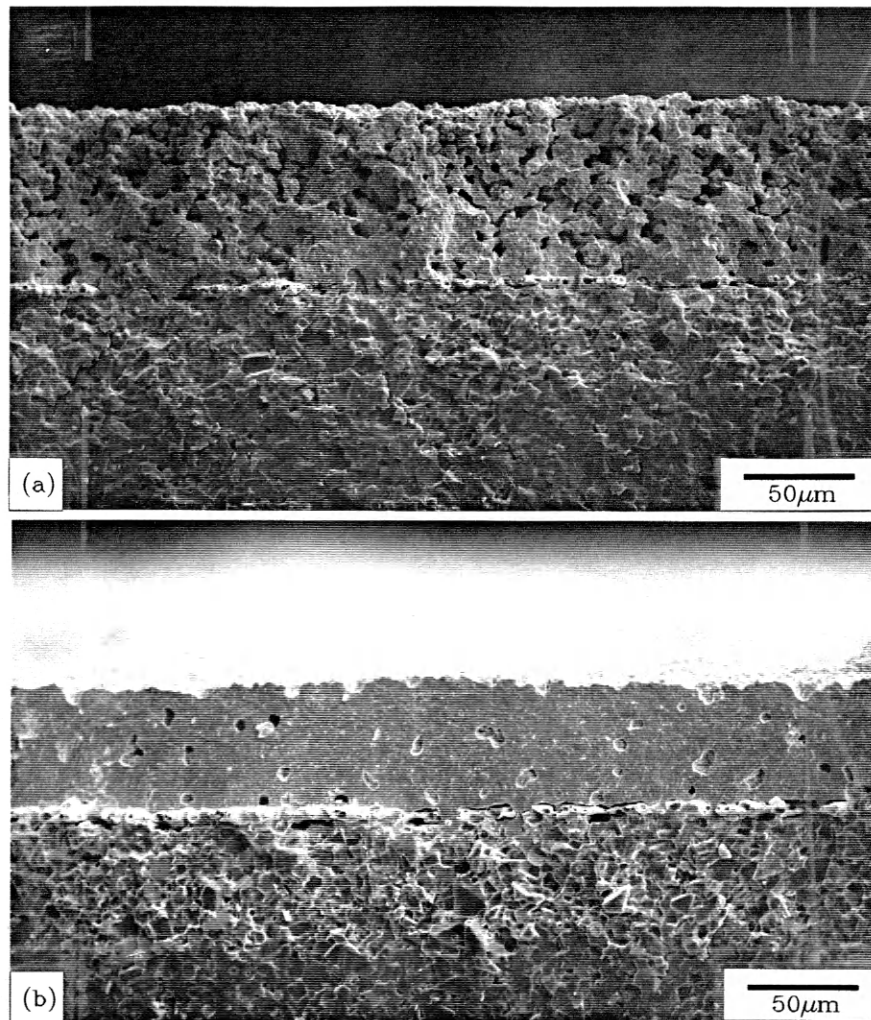


Figure 4.27 SEM micrographs of the fractured cross sections of thick film samples fired at 850°C for 10 minutes with a heating rate of 580°C/min; a) PMN - PT + 20wt% PGS + 5wt% PbO b) PMN - PT + 30wt% PGS + 5wt% PbO. The thick film layers are shown on the top of the photos with the alumina substrate on the bottom.

film PMN - PT samples with PGS and PbO additions heat-treated at 850°C for 10 minutes with a heating rate of 580°C/min. The PMN - PT materials densified to the closed porosity with 30 weight percent PGS and 5 weight percent PbO additions at 850°C even with short sintering time and very fast heating rate (10 minutes, 580°C/min). Also, the PMN - PT with 30 weight percent PGS addition densified to the closed porosity at the same heating condition above. This indicates that the PMN - PT materials densify by liquid phase sintering of PGS addition.

The effect of PbO additions on the densification of the samples is shown in Figure 4.28. The PMN - PT materials did not densify to the closed porosity with 5, 10, or 20 weight percent PbO addition at 850°C. This indicates that there is no significant effect on the densification behavior of PMN - PT with PbO addition in thick film samples fired at 850°C.

4.2.2 X-ray Diffraction(XRD)

Figure 4.29 shows the x-ray diffraction patterns of the surface of PMN - PT with 30 weight percent PGS addition thick film samples fired at 800, 850, and 900°C for ten minutes with a heating rate of 580°C/min. The amount of the pyrochlore phase increased with increasing firing temperatures, and became dominant firing at 900°C.

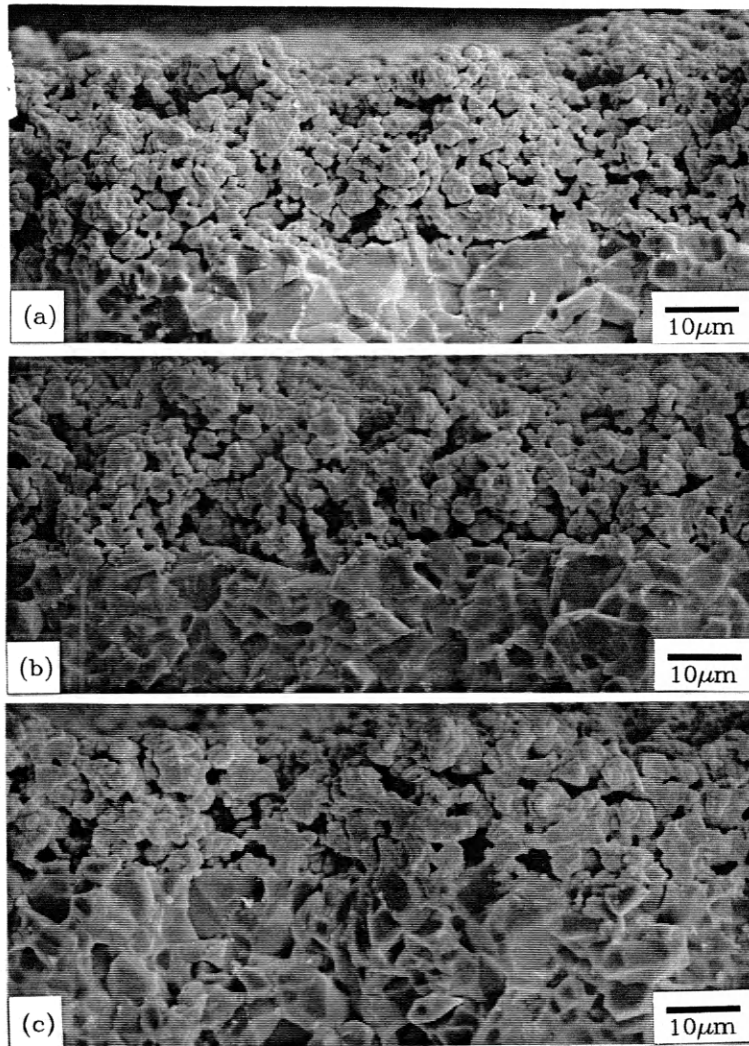


Figure 4.28 SEM micrographs of the fractured cross sections of thick film samples fired at 850°C for 10 minutes with a heating rate of 580°C/min; a) PMN - PT + 5wt% PbO b) PMN - PT + 10wt% PbO c) PMN - PT + 20wt% PbO. The thick film layers are shown on the top of the photos with the alumina substrate on the bottom.

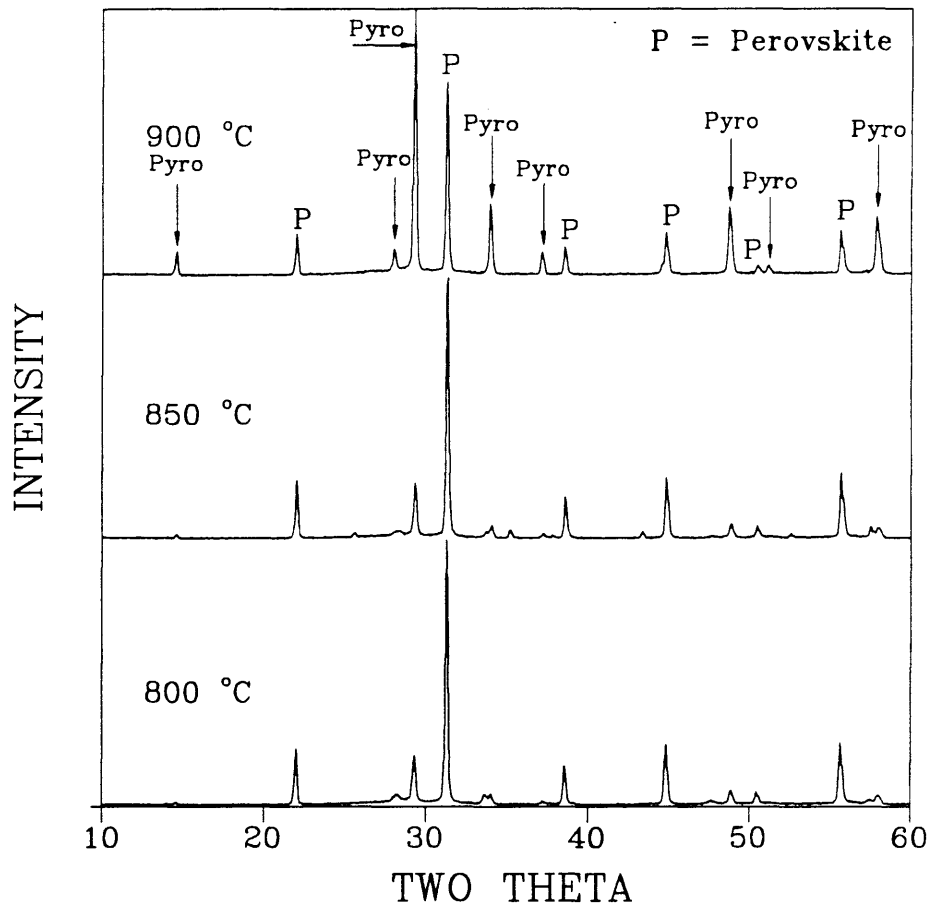


Figure 4.29 X-ray diffraction patterns of the surface of PMN - PT + 30wt% PGS thick film samples fired at 800, 850, and 900°C for 10 minutes with a heating rate of 580°C/min. The peaks in the top pattern are labeled with P for PMN - PT perovskite, and Pyro for $Pb_3Nb_4O_{13}$ pyrochlore.

Figure 4.30 shows the effect of sintering time on the formation of the pyrochlore phase of PMN - PT thick film samples with 30 weight percent PGS addition. The amount of the pyrochlore phase increases with increasing sintering time. Most of the perovskite phase converts to the pyrochlore phase by firing at 850°C for sixty minutes.

The effect of heating rate on the formation of the pyrochlore phase is shown in Figure 4.31. The amount of the pyrochlore phase decreases with increasing heating rate. However, the formation of the pyrochlore phase was not eliminated even with a heating rate of 580°C/min.

X-ray diffraction patterns of PMN - PT samples with and without PGS addition fired at 900°C for ten minutes with a heating rate of 580°C/min are shown in Figure 4.32. Without PGS addition (bottom pattern in Figure 4.32) the pyrochlore phase was not observed. However, with PGS addition to PMN - PT the perovskite phase partially converted to the pyrochlore phase. This is possibly due to the removal of lead from the PMN - PT by the PGS, which causes the lead deficient pyrochlore phase to form. The amount of pyrochlore phase increased with increasing PGS addition.

Figure 4.33 shows the x-ray diffraction patterns of PMN - PT with 30 weight percent PGS and 5 weight percent PbO additions heat-treated at 850°C for ten and thirty minutes

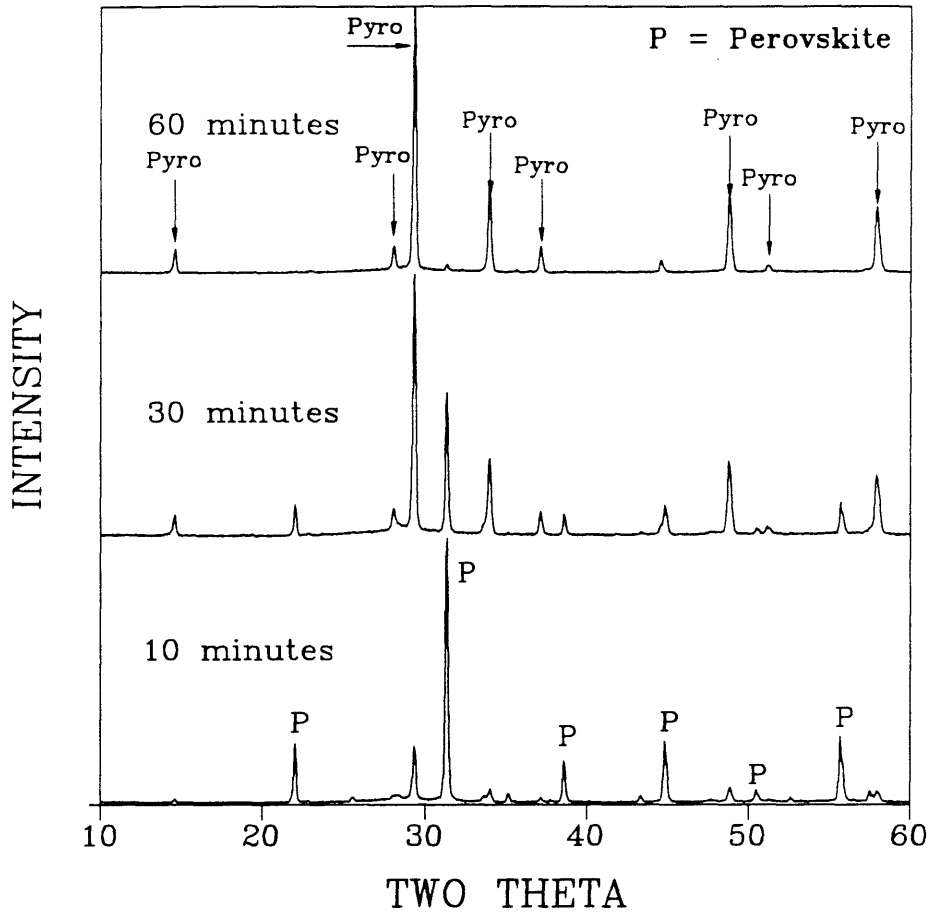


Figure 4.30 X-ray diffraction patterns of the surface of PMN - PT + 30wt% PGS thick film samples fired at 850°C for 10, 30, and 60 minutes with a heating rate of 580°C/min. The peaks in the bottom pattern are labeled with P for PMN - PT perovskite, and Pyro for $Pb_3Nb_4O_{13}$ pyrochlore in the top pattern.

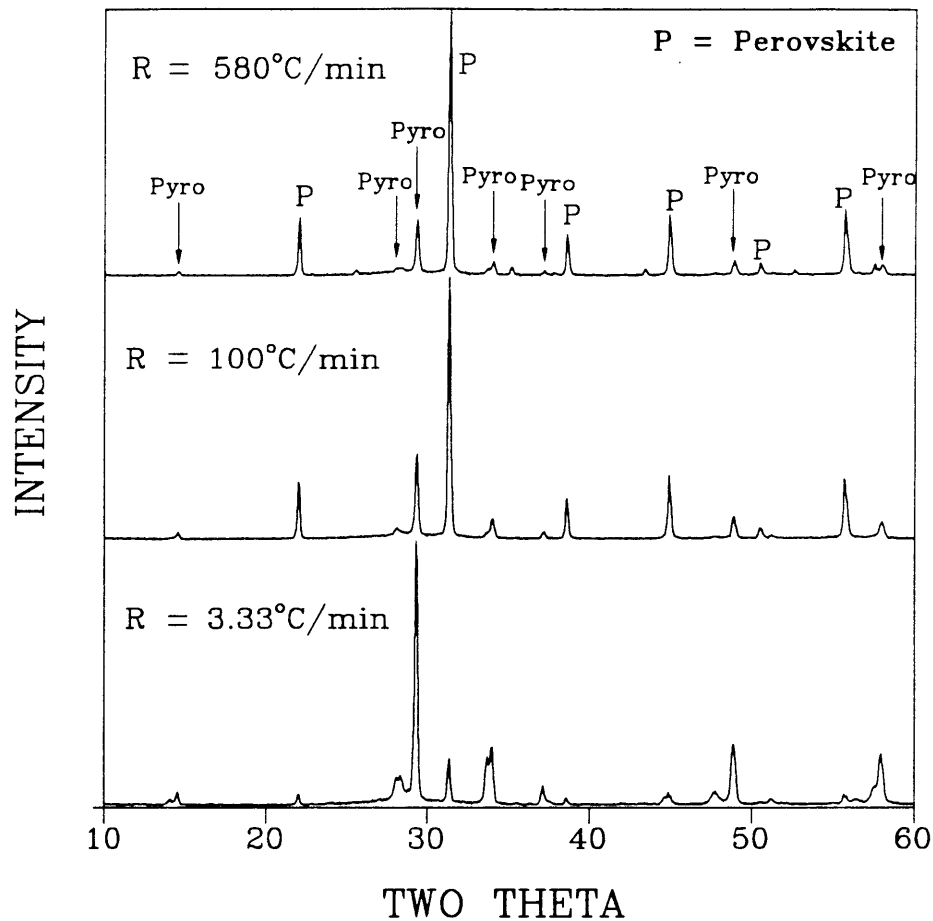


Figure 4.31 X-ray diffraction patterns of the surface of PMN - PT + 30wt% PGS thick film samples fired at 850°C for 10 minutes with a heating rate of 3.33°C/min, 100°C/min, and 580°C/min. The peaks in the top pattern are labeled with P for PMN - PT perovskite, and Pyro for $Pb_3Nb_4O_{13}$ pyrochlore.

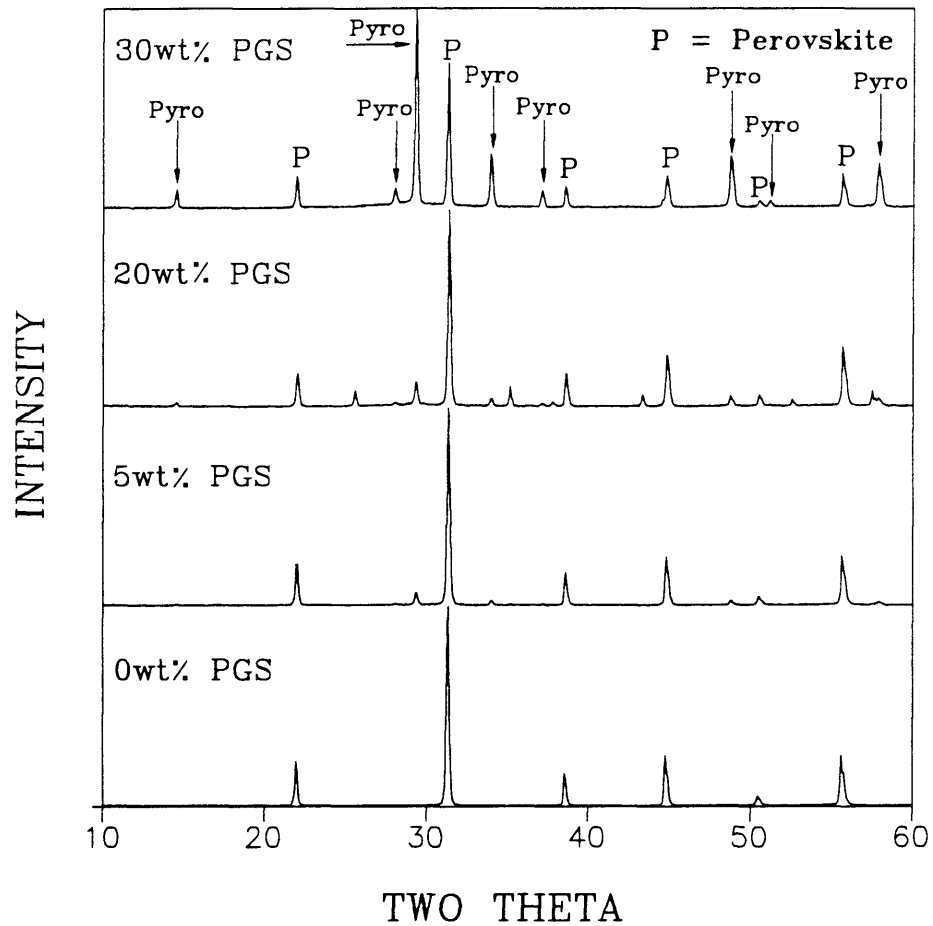


Figure 4.32 X-ray diffraction patterns of the surface of PMN - PT with 0, 5, 20, and 30wt% PGS addition thick film samples fired at 900°C for 10 minutes with a heating rate of 580°C/min. The peaks in the top pattern are labeled with P for PMN - PT perovskite, and Pyro for $Pb_3Nb_4O_{13}$ pyrochlore.

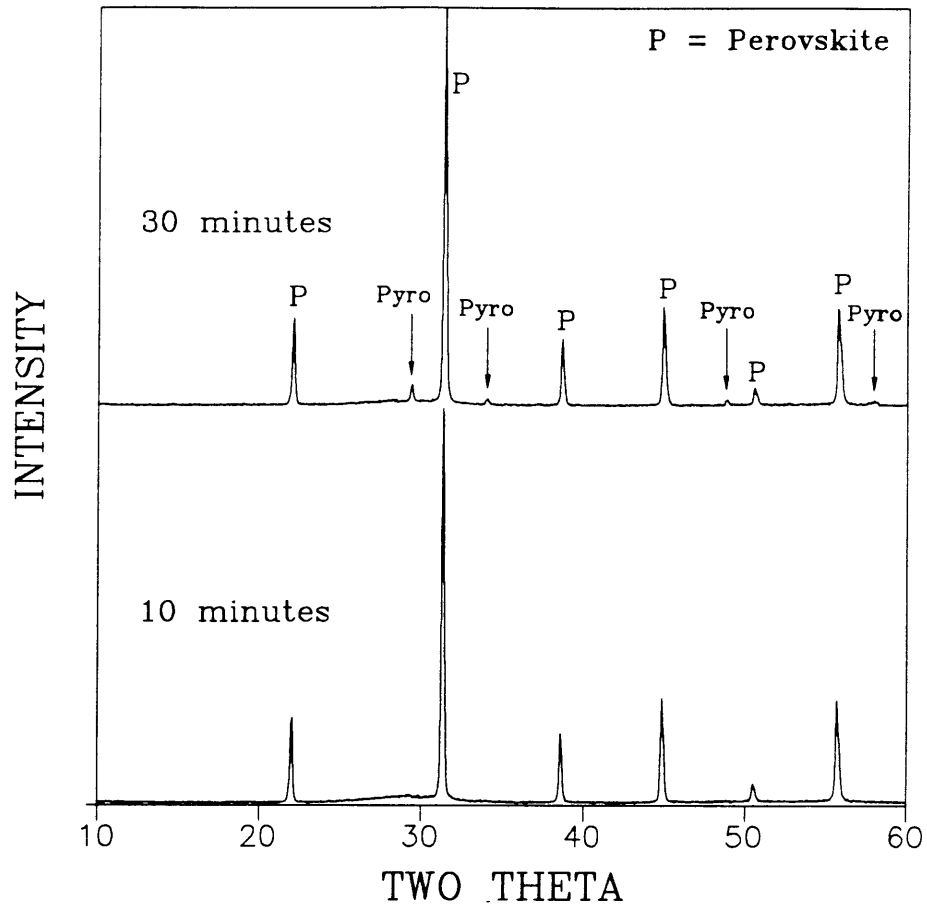


Figure 4.33 X-ray diffraction patterns of the surface of PMN - PT + 30wt% PGS + 5wt% PbO thick film samples fired at 850°C for 10 and 30 minutes with a heating rate of 580°C/min. The peaks in the top pattern are labeled with P for PMN - PT perovskite, and Pyro for $Pb_3Nb_4O_{13}$ pyrochlore.

with a heating rate of 580°C/min. The excess PbO addition to PMN - PT + PGS composition significantly reduces the formation of the pyrochlore phase (compare Figure 4.30 with 4.33). No pyrochlore peaks were observed after firing at 850°C for ten minutes. However, increasing the sintering time caused the pyrochlore phase to form.

4.2.3 Dielectric Properties

Figure 4.34 shows the dielectric constant and dissipation factor plotted versus temperature at five low field frequencies for a thick film sample of PMN - PT with 30 weight percent PGS and 5 weight percent PbO fired at 850°C for ten minutes with a heating rate of 580°C/min. Figure 4.35 shows the fractured cross section of this sample. These figures show that the PMN - PT with 30 weight percent PGS and 5 weight percent PbO composition densified to the closed porosity in thick film form with a 1 KHz, room temperature dielectric constant value of about 1500 and dissipation factor less than 6%. These results indicate the potential of achieving high dielectric constant thick film capacitor compositions that densify to closed porosity in typical thick film firing profiles, and thus not require an encapsulant. The commercially available thick film compositions require encapsulants, because of poor

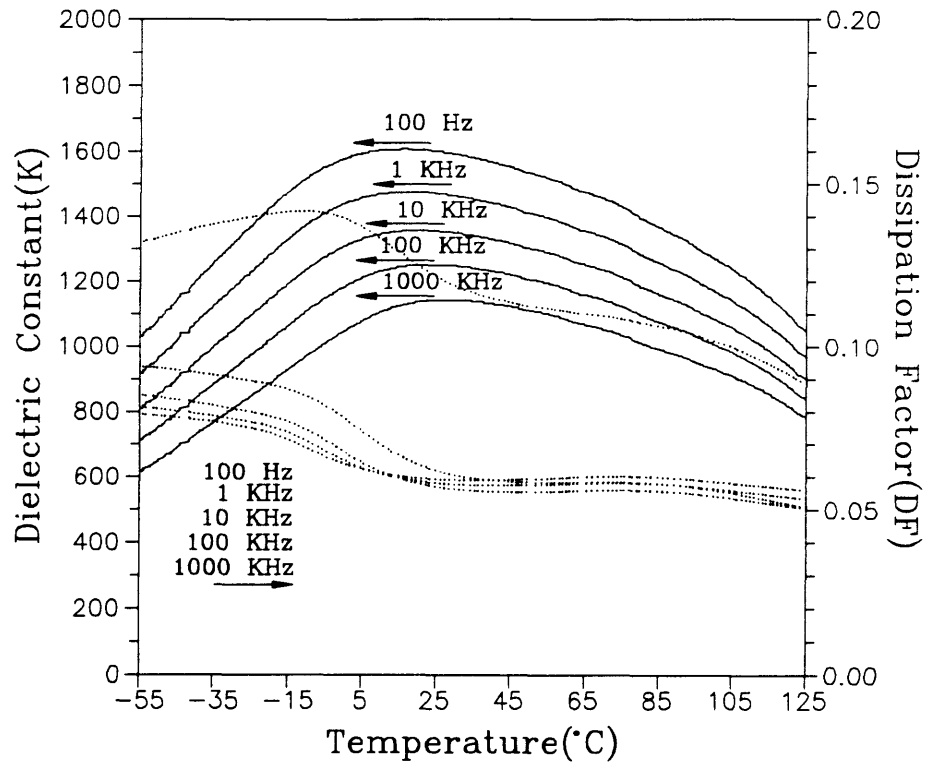


Figure 4.34 The dielectric constant and dissipation factor of a thick film sample of PMN - PT with 30wt% PGS and 5wt% PbO fired at 850°C for 10 minutes with a heating rate of 580°C/min plotted versus temperature for five frequencies.

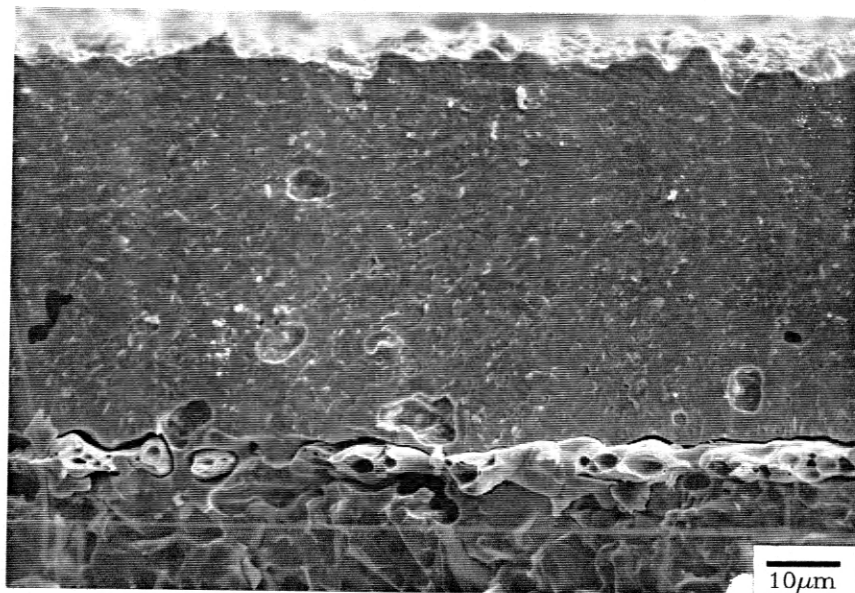


Figure 4.35 SEM micrographs of a fractured cross section of a thick film sample of PMN - PT with 30wt% PGS and 5wt% PbO fired at 850°C for 10 minutes with a heating rate of 580°C/min. The thick film dielectric layer is shown on the top of the photo with the Pt conductor shown at the bottom of the dielectric layer.

densification behavior.

The densification behavior and electrical properties for four different compositions in thick film form are summarized in the Table 4.4. The dielectric constant decreases with increasing PGS addition, however 30 weight percent PGS is required to produce closed porosity. The dissipation factor and conductivity of the composition with 20 weight percent PGS and 10 weight percent PbO are significantly higher than the other compositions apparently because of the large additions of PbO and PGS. For the electrical property measurement, the bottom Pt electrode was first printed and fired on the alumina substrate at 1300°C for one hour, followed by five double layers of dielectric, and then the top electrode was formed by sputtering with Au. These electrodes were used to reduce interaction with the dielectrics.

Figures 4.36 a) and b) show the fractured cross sections of PMN - PT with 30 weight percent PGS and 5 weight percent PbO samples prepared with two commercial thick film conductors; silver (Dupont 6160) and silver/palladium (Dupont 6134). The bottom electrode was first printed and fired on the alumina substrate at 850°C for ten minutes with a heating rate of 580°C/min, and then five double layers of dielectric were printed and fired. Finally the top

Table 4.4 The summary of the densification behavior and electrical properties of four different thick film compositions fired at 850°C for 10 minutes with a heating rate of 580°C/min.

| | PMN-PT + 30wt% PGS + 5wt% PbO | PMN-PT + 20wt% PGS + 5wt% PbO | PMN-PT + 20wt% PGS + 10wt% PbO | PMN-PT + 5wt% PGS + 10wt% PbO |
|---|---|---|--|---|
| Densification | Closed porosity | Open/Closed porosity(?) | Open/Closed porosity(?) | Open porosity |
| Dielectric Constant (K_{max} at 1 KHz) | ≈ 1500 | ≈ 1700 | ≈ 2200 | ≈ 2600 |
| Capacitance change (-30 ~ 85°C) | < 20% | < 30% | < 20% | < 36% |
| EIA Characteristic* | Y5S | Y5T | Y5S | Y5U |
| Dissipation Factor (1 KHz, 25°C) | < 6% | < 5% | < 12% | < 6% |
| Resistivity (100V, 25°C) | > 10 ¹⁰ Ohm-cm | > 10 ¹⁰ Ohm-cm | > 10 ⁸ Ohm-cm | > 10 ¹⁰ Ohm-cm |

* See Appendix A

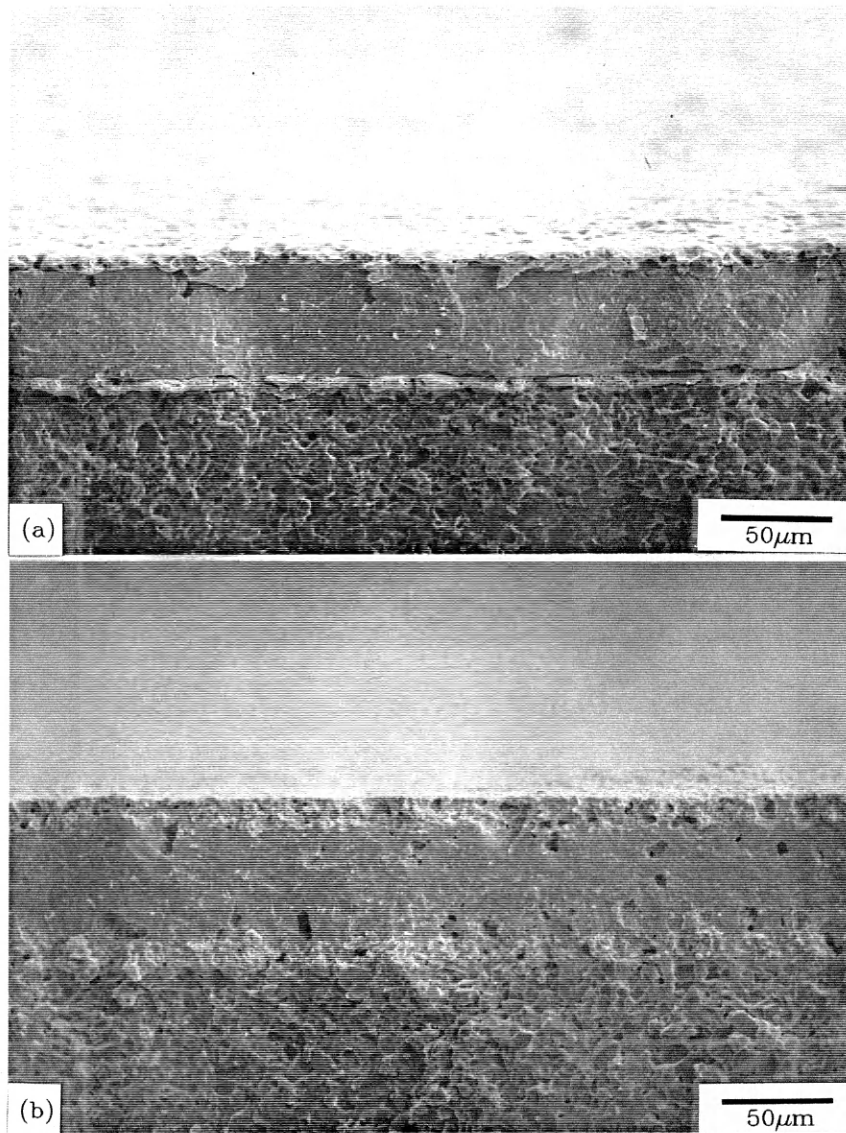


Figure 4.36 SEM micrographs of the fractured cross sections of thick film PMN - PT with 30wt% PGS and 5wt% PbO samples fired at 850°C for 10 minutes with a heating rate of 580°C/min; a) fired with silver electrode (Dupont 6160) b) fired with silver/palladium electrode (Dupont 6134).

electrode was printed and fired. These commercial thick film pastes also contain other inorganic additives in addition to the metal to assist in densification and to improve properties. These additives may interact with the dielectric degrading properties. Figure 4.36 shows that the dielectric densified well with the silver electrode(a), but not with the silver/palladium electrode(b). The electrical properties could only be measured with the silver electrodes, because the samples with the silver/palladium electrodes electrically shorted.

Figure 4.37 shows the dielectric constant and dissipation factor plotted versus temperature at five low field frequencies for the sample fired with silver electrodes (Dupont 6160). The maximum dielectric constant was greater than 800 with a dissipation factor less than 3% at 1 KHz. The dielectric constant and dissipation factor values are lower than that of the sample with a fired Pt bottom electrode and a sputtered Au top electrode. Complicated interactions occur with these different electrode materials, and thus additional research is needed to understand the changes in the dielectric properties that occur.

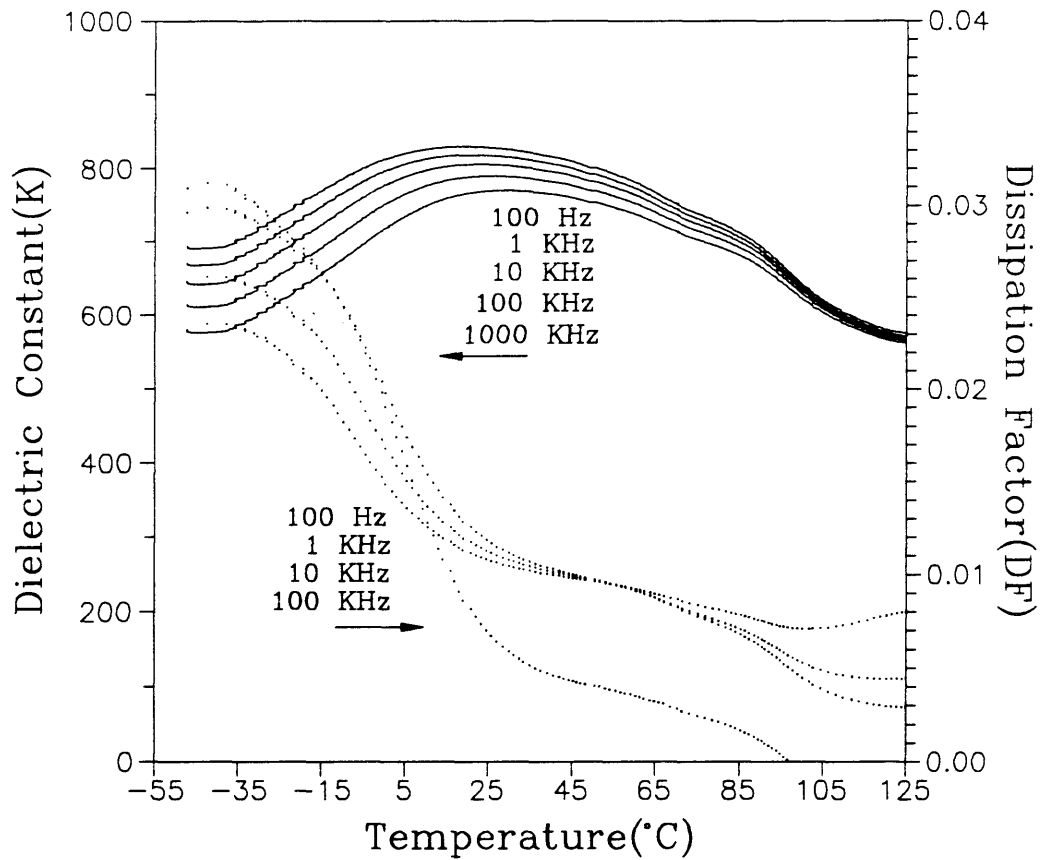


Figure 4.37 The dielectric constant and dissipation factor of a PMN - PT with 30wt% PGS and 5wt% PbO thick film sample fired with silver electrodes (Dupont 6160) at 850°C for 10 minutes with a heating rate of 580°C/min plotted versus temperature for five frequencies.

CHAPTER 5

CONCLUSION

The summary and conclusions of this research are divided in two sections: bulk samples and thick film samples.

5.1 Bulk Samples

The particle size distribution and morphologies of the starting powders were found to be controlled by the ball milling conditions. The reduction in particle size has a significant effect on increasing the density of fired samples. The densities of the bulk samples, with and without PGS additions, increased with increasing firing temperature and time. Bulk samples of PMN - PT with 5 weight percent PGS addition densified to 93 percent of the theoretical density at 850°C for one hour, while those without PGS densified to only 84 percent of the theoretical density.

From x-ray diffraction, the $\text{Pb}_5\text{Ge}_2\text{SiO}_{11}$ additions to PMN - PT resulted in the formation of lead rich $\text{Pb}_3\text{Ge}_{2/3}\text{Si}_{1/3}\text{O}_5$.

The $\text{Pb}_5\text{Ge}_2\text{SiO}_{11}$ additions appear to remove lead oxide from the PMN - PT to form the lead rich $\text{Pb}_3\text{Ge}_{2/3}\text{Si}_{1/3}\text{O}_5$ phase. The formation of this PGS phase involves an increase in lead oxide content which promotes the formation of a lead deficient pyrochlore phase ($\text{Pb}_3\text{Nb}_4\text{O}_{13}$).

The grain size of the PMN - PT was increased with increasing firing temperature and time. However, with the addition of PGS, the firing temperature and time did not significantly affect the grain size. Also, the average grain size of the PMN - PT without PGS addition was larger than those with the addition of PGS.

From the dielectric measurements and SEM micrographs, the dielectric constant of PMN - PT samples without PGS addition generally increased with increasing firing temperature and time due to the grain growth and increased density. The dissipation factor slightly increased with increasing PGS addition. The dielectric constant was reduced by the formation of a diphasic composite of low dielectric constant PGS with high dielectric constant PMN - PT. The limited grain growth of PMN - PT by the PGS addition, and the formation of pyrochlore may have also decreased the dielectric constant.

5.2 Thick Film Samples

The PMN - PT samples in thick film form did not densify at 850°C even with 20 weight percent PGS addition. This is because of the constrained sintering by the substrate in the parallel directions to the substrate. Thick film PMN - PT densified to closed porosity with 30 weight percent PGS and 5 weight percent PbO additions at 850°C in only ten minutes sintering time with a heating rate of 580°C/min. The excess PbO addition did not significantly affect the densification of PMN - PT materials in thick film form firing at 850°C for ten minutes.

In thick film, the amount of pyrochlore phase was increased with increasing firing temperature and time, and decreased with increasing heating rate. The PGS addition to PMN - PT caused the perovskite phase to convert to pyrochlore. Excess PbO addition to PMN - PT with PGS additions prevented the formation of the pyrochlore phase.

Thick film PMN - PT with 30 weight percent PGS and 5 weight percent PbO additions densified to close porosity firing at 850°C for ten minutes with a room temperature dielectric constant greater than 1500 and dissipation factor less than 6% at 1 KHz. This combination of good densification behavior and high dielectric constant is currently not commercially available in thick film form. In

addition, preliminary results indicate that these compositions are compatible with a commercial pure silver thick film conductor paste (Dupont 6160).

CHAPTER 6

RECOMMENDATIONS FOR FUTURE RESEARCH

The following areas may be interesting for future research to further understand the densification behavior and dielectric properties of PMN - PT / PGS systems for thick film capacitor applications.

1. Optimization and reduction of the amount of PGS and PbO additions to the PMN - PT materials to enhance the physical and electrical properties.
2. Investigate the compatibility of the PMN - PT / PGS / PbO system with commercialized thick film conductors, and the pure metal electrode pastes.
3. Experimentally evaluate the reliability of the optimized thick film samples.
4. Investigate the dielectric property differences between the PMN materials prepared from Pb_3O_4 and PbO.

REFERENCE

1. S. J. Jang, W. A. Schulze and J. V. Biggers, "Low-Firing Capacitor Dielectrics in the System $\text{Pb}(\text{Fe}_{2/3}\text{W}_{1/3})\text{O}_3\text{-Pb}(\text{Fe}_{1/2}\text{Nb}_{1/2})\text{O}_3\text{-Pb}_5\text{Ge}_3\text{O}_{11}$ ", Ceram. Bull., Vol. 62 (2), pp. 216-218 (1983).
2. T. R. Shrout and A. Halliyal, "Preparation of Lead-Based Ferroelectric Relaxors for Capacitors", Am. Ceram. Soc. Bull., Vol. 66 (4), pp. 704-711 (1987).
3. M. Yonezawa, "Low-Firing Multilayer Capacitor Materials", Ceram. Bull., Vol. 62 (12), pp. 1375-1383 (1983).
4. Yonezawa et al., "Ceramic Compositions Having High Dielectric Constant", U. S. Patent No. 4,078,938 Mar. (1978).
5. Yonezawa et al., "Ceramic Compositions", U. S. Patent No. 4,236,928 Dec. (1980).
6. D. A. Payne and S. M. Park, "Heterophasic Ceramic Composition", U. S. Patent No. 4,218,723 Aug. (1980)
7. Park et al., "Ceramic Composition for Dielectric in Multilayer Capacitors", U. S. Patent Oct. (1985).
8. S. L. Fu and G. F. Chen, "Low Firing Thick Film Dielectrics in the System $\text{Pb}(\text{Fe}_{2/3}\text{W}_{1/3})_x(\text{Fe}_{1/2}\text{Nb}_{1/2})_{0.86-x}\text{Ti}_{0.14}\text{O}_3\text{-Bi}_2\text{O}_3/\text{Li}_2\text{O}$ ", Am. Ceram. Soc. Bull., Vol. 66 (9), pp. 1397-1400 (1987).
9. T. Yasumoto, N. Iwase and M. Harata, "High Dielectric Constant Thick Film Capacitors Fireable in Air and Nitrogen Atmosphere", The Int. J. for Hybrid Microelectronics, Vol. 12 (3), pp. 156-161 (1989).
10. T.C. Reiley, J. V. Badding, D. A. Payne and D. A. Chance, "A Low-Temperature Firing Thick Film Capacitor Material Based on Lead Iron Niobate/Tungstate", Mat. Res. Bull., Vol. 19, pp. 1543-1549 (1984).

11. C. A. Randall, A. D. Hilton, D. J. Barber and T. R. Shrout, "Extrinsic Contributions to the Grain Size Dependence of Relaxor Ferroelectric $\text{Pb}(\text{Mg}_{1/3}\text{Nb}_{2/3})\text{O}_3$: PbTiO_3 Ceramics", J. Mater. Res., Vol. 8 (4), pp. 880-884 (1993).
12. J. Collier, I. V. Cornejo and M. J. Haun, "Ferroelectric Thick-Films for Piezoelectric Applications", To Be Published in Ferroelectrics.
13. G. H. Haertling, "Piezoelectric and Electrooptic Ceramics", pp. 139-225 in Ceramic Materials for Electronics, edited by R. C. Buchanan, Marcel Dekker, Inc., New York (1986).
14. L. E. Cross, "Relaxor Ferroelectrics", Ferroelectrics, Vol. 76, pp. 241-267 (1987).
15. D. J. Voss, S. L. Swartz and T. R. Shrout, "The Effect of Various B-Site Substitutions on The Dielectric Properties of $\text{PbMg}_{1/3}\text{Nb}_{2/3}\text{O}_3$ Ceramics, Ferroelectrics, Vol. 50, pp. 203-208 (1983)
16. G. A. Smolenskii and V. A. Isupov, "Phase Changes of Certain Solid Solutions Having Electrical Properties of Rochelle Salt", Dokl. Akad. Nauk SSSR, Vol. 96, pp. 53-54 (1954).
17. N. Setter and L. E. Cross, "The Contribution of Structural Disorder to Diffuse Phase Transitions in Ferroelectrics", J. Mat. Sci., Vol. 15, pp. 2478-2482 (1980).
18. N. Setter and L. E. Cross, "The Role of B-Site Cation Disorder in Diffuse Phase Transition Behavior of Perovskite Ferroelectrics", J. Appl. Phys., Vol. 51 (8), pp. 4356-4360 (1980).
19. G. A. Smolenskii and A. I. Agranovskaya, "Dielectric Polarization and Losses of Some Complex Compounds", Sov. Phys. Tech. Phys., Vol. 3, pp. 1380-1382 (1958).
20. S. L. Swartz and T. R. Shrout, "Fabrication of Perovskite Lead Magnesium Niobate", Mat. Res. Bull., Vol. 17, pp. 1245-1250 (1982).

21. J. P. Guha, "Comment on Dielectric Properties of Lead-Magnesium Niobate Ceramics", J. Am. Ceram. Soc., Vol. 68 (3), pp. C-86-C-87 (1985).
22. J. P. Guha and H. U. Anderson, "Preparation of Perovskite $\text{Pb}(\text{Mg}_{1/3}\text{Nb}_{2/3})\text{O}_3$ Using $\text{Pb}_3\text{Nb}_2\text{O}_8$ and MgO ", J. Am. Ceram. Soc., Vol. 69 (11), pp. C-287-C-288 (1986).
23. D. H. Kang and K. H. Yoon, "Dielectric Properties due to Excess PbO and MgO in Lead Magnesium Niobate Ceramics", Ferroelectrics, Vol. 87, pp. 255-264 (1988).
24. M. Lejeune and J. P. Boilot, "Formation Mechanism and Ceramic Process of the Ferroelectric Perovskites: $\text{Pb}(\text{Mg}_{1/3}\text{Nb}_{2/3})\text{O}_3$ and $\text{Pb}(\text{Fe}_{1/2}\text{Nb}_{1/2})\text{O}_3$ ", Ceram. Int., Vol. 8 (3), pp. 99-103 (1982).
25. H. S. Horowitz, "Low-Temperature Synthesis Route to MgNb_2O_6 ", J. Am. Ceram. Soc., Vol. 71 (5), pp. C-250-C-251 (1988).
26. E. Goo, "Microstructure of Lead-Magnesium Niobate Ceramics", J. Am. Ceram. Soc., Vol. 69 (8), pp. C-188-C-190 (1986).
27. V. A. Bokov and I. E. Mylnikova, "Electrical and Optical Properties of Single Crystals of Ferroelectrics with a Diffuse Phase Transition", Sov. Phy. Solid State, Vol. 3 (3), pp. 613-623 (1961).
28. G. A. Smolenskii and A. I. Agranovskaya, "Dielectric Polarization of a Number of Complex Compounds", Sov. Phy. Solid State, Vol. 1 (10), pp. 1429-1437 (1959).
29. G. A. Smolenskii, V. A. Isupov, A. I. Agranovskaya and S. N. Popov, "Ferroelectrics with Diffuse Phase Transitions", Sov. Phys. Solid State, Vol. 2 (11), pp. 2584-2594 (1961).
30. T. R. Shrout, U. Kumar, M. Megherhi, N. Yang and S. J. Jang, "Grain Size Dependence of Dielectric and Electrostriction of $\text{Pb}(\text{Mg}_{1/3}\text{Nb}_{2/3})\text{O}_3$ - Based Ceramics", Ferroelectrics, Vol. 76, pp. 479-487 (1987).

31. J. Chen, A. Gorton, H. A. Chan and M. P. Harmer, "Effect of Powder Purity and Second Phases on the Dielectric Properties of Lead Magnesium Niobate Ceramics", J. Am. Ceram. Soc., Vol. 69 (12), pp. C-303-C-305 (1986).
32. S. L. Swartz, T. R. Shrout, W. A. Schulze and L. E. Cross, "Dielectric Properties of Lead-Magnesium Niobate Ceramics", J. Am. Ceram. Soc., Vol. 67 (5), pp. 311-315 (1984).
33. Y. Yamashita, "Relaxor Materials (Past, Present and Future)", The 6th US-JAPAN Seminar on Dielectric and Piezoelectric Ceramics, Maui, Hawaii, Nov.11-12, 1993
34. J. Wilson, J. Arthur and T. Jaenecke, "Advancing the State-of-the-Art in MLCC Fabrication", Ceramic Industry, pp. 51-56 (Sep. 1993).
35. R. L. Brown, "LTCC Provides an Integrated Approach to Multichip Module Design", Electronic Packaging & Production, PP. 38-40 (Oct. 1993).
36. J. Steinberg and B. Kistler, "Materials and Applications for Thick Film RC Networks", 1990 Proceedings of the International Symposium on Microelectronics, pp. 276-284, International Society for Hybrid Microelectronic, Virginia.
37. M. Rusinko, "Dielectric Mixing in the PLZT-Pb₅Ge₃O₁₁ System", B. Sc. Thesis, Penn. State. University, University PARK, pa., May 1975.
38. W. A. Schulze and J. V. Biggers, "Piezoelectric Properties of Pb₅Ge₃O₁₁ Bonded PZT Composites", Mat. Res. Bull., Vol. 14, pp. 721-730 (1979).
39. D. A. Payne and S. M. Park, "Heterophasic Ceramic Capacitor", U. S. Patent No. 4,158,219 Jun. (1979).
40. D. A. Payne, S. M. Park and O. C. Jahnke, " Method of Producing Internal Boundary Layer Ceramic Compositions", U. S. Patent No. 4,237,084 Dec. (1980).

APPENDIX A

Temperature Coefficient of Capacitance(TCC) Category*

| Code | Temperature Range(°C) |
|------|-----------------------|
| X7 | -55 to 125°C |
| X5 | -55 to 85°C |
| Y5 | -30 to 85°C |
| Z5 | 10 to 80°C |

| Code | Change from R.T Capacitance |
|------|-----------------------------|
| D | ± 3.3% |
| E | ± 4.7% |
| F | ± 7.5% |
| P | ± 10% |
| R | ± 15% |
| S | ± 22% |
| T | + 22 to -33% |
| U | + 22 to -56% |
| V | + 22 to -82% |

*Established by Electronics Industry Association(EIA)